THE STRUCTURE OF GIANT EXTRAGALACTIC HII REGIONS

Thesis by

Jorge Melnick

In Partial Fulfillment of the Requirements

for the Degree of

Doctor of Philosophy

California Institute of Technology

Pasadena, California

1977

Submitted November 8, 1976

To

Professor Claudio Anguita, Director
of the Chilean National Observatory
who has kept burning the flame of
Chilean astronomy against the
strongest winds and the heaviest rains.
You have carved the road Claudio; I
hope we can together pave it.

Caminante no hay caminos
se hace camino al andar.
Golpe a golpe, verso a verso.

(Machado)

ACKNOWLEDGEMENT

I would like to thank the many people who in multiple ways contributed to make my stay at Caltech more enjoyable. It is not possible to name everyone but I haven't forgotten you all.

I wish to thank Dr. Guido Münch, my thesis advisor, for his warm guidance during the past four years, and in particular for his indispensable advice and support during the preparation of this thesis. He has set for me the highest example of how scientific research should be done and I hope to keep my own work up to this high standard.

Dr. Wallace Leslie William Sargent was the first person ever to ask me if I liked Pasadena. He has since asked me the same question many times but only that first time was my answer yes. For your concern and advice, thank you Wal.

I would like to express my sincere gratitude to Dr. James Gunn for sharing his contagious enthusiasm for astronomy and for his friendliness and his advice and support during the whole course of my stay at Caltech.

I am grateful to Dr. Victor Blanco and to Dr. Jesse Greenstein for the award of an AURA Fellowship which allowed me to come to Caltech.

I have benefited a great deal from the friendliness of many fellow graduate students at Caltech. In particular

I would like to thank: John Hoessel for many hours of conversation and for sharing some observational ventures; Stephen Kent who, in addition to providing some very helpful discussions regarding parts of this thesis, provided a long series of conversations about astronomy, philosophy, politics and the importance of Wonder "Bread" in the welfare of rats. The Knights of the Round Pinochle Table-Sir Arthur Huchra, Sir Galahad Elias and Sir Lancelot Williams-provided a great deal of friendship at the Robinson "engine room". Fortunately, I never learned how to play the game.

I would like to thank John Kormendy for many helpful discussions regarding this thesis and a multiplicity of other astronomical problems. I also thank him for his now legendary recipe for the water-vinegar-honey punch.

My thanks to Larry Blakee and Bud Smith for the most cheerful and friendly help with the Palomar electronics, and to Chip Williams who, despite his habit of polluting the dome with his yellow "truck", provided efficient assistance at the telescope. I am also grateful to Earle Emery for his skill and his incredible patience in making some parts I badly needed for my observing runs.

My special thanks to Lilo Hauck for her everlasting friendliness and for her supersonic efficiency in solving more than one administrative problem. I also thank

Marilynne Rice for typing a goodly portion of the first draft of this thesis and all the references of the final version.

I have no words to thank Margaret Katz for carefully reading and checking the complete manuscript, and for translating my "Chileanglish" into legible "Brooklyneese". Thank you again, Margaret.

Last, but by no means least, I would like to express my love and gratitude to Helen Holloway. There are so many different reasons to thank her that I'll just say: Thank you Helen, thank you for being you.

ABSTRACT

The existence of a close correlation between the linear diameters of giant HII regions in late type spiral and irregular galaxies and the width of their global H_α emission is demonstrated by means of line profiles obtained using interferometric techniques. The relation (diameter-line width) established in members of the local and M81 – NGC 2403 groups is applied to a redetermination of the distance to M101.

With the purpose of avoiding the difficulties involved in accurately determining linear diameters of giant HII regions, a correlation between H_β luminosity and line profile width has been established. The dust distribution in giant HII regions, which is the factor limiting the possible application of the (H_β luminosity-line width) relation to the determination of distances, is studied in considerable detail. It is found that most of the extinction affecting the nebular light comes from dust particles that are mixed with the ionized gas, and that the wavelength dependence of the dust absorption is similar to, but significantly different from Whitford's extinction law.

A dynamical model for giant HII regions is constructed on the basis of a detailed study of the 30 Doradus nebula in the LMC. It is shown that giant HII regions can be regarded as aggregates or "clusters" of small HII regions surrounding the hundreds of O-B stars which ionize the giant

nebulae. The highly supersonic velocities observed in these giant HII complexes, therefore, are interpreted as reflecting the motions of the individual stars imbedded therein. It is also shown that galactic shear, amplified during the gravitational collapse of the interstellar cloud out of which the HII regions were formed, can account for at least part of the observed motions.

TABLE OF CONTENTS

	Preliminary Remarks	1
Part I.	Velocity Dispersions in Giant HII Regions	2
	I. Introduction	3
	II. Observations	4
	III. Discussion	7
	References	12
Part II.	The (Linear Diameter – Luminosity) Relation for Giant Extragalactic HII Regions	19
	I. Introduction	20
	II. Observations	22
	III. Results	32
	IV. Conclusions	42
	V. Summary	44
	References	50
Part III.	The Structure of the 30 Doradus Nebula	66
	I. Introduction	67
	II. Observations	71
	III. Discussion	79
	IV. Dynamics	98
	V. Concluding Remarks	109
	References	120

PRELIMINARY REMARKS

This Thesis is divided into three parts, each in the form of a paper submitted to the Astrophysical Journal. Each part is independently readable and forms a separate unit in which different aspects of the nature of giant extragalactic HII regions are considered. A special effort has been made to avoid redundancy and at the same time to maintain the coherence of each paper. However, Papers I and II form the basis of the discussion presented in Paper III. Some repetition has been unavoidable, particularly in the description of the observations and the data reduction techniques.

The observations reported in Papers I and II were obtained almost a year and a half after the observations of 30 Doradus had been secured. Thus, we have not addressed ourselves to some questions raised in Papers I and II that could be answered on the basis of further observations of 30 Doradus.

Paper I is presented in the form accepted for publication in the Astrophysical Journal.

PART I

VELOCITY DISPERSIONS IN GIANT HII REGIONS

I. INTRODUCTION

The linear sizes of the giant HII regions in late type spiral galaxies have been shown by Sandage and Tammann (1974a) to correlate well with the luminosity class L_C of the parent galaxy. In the course of studying the structure of such HII regions it has been noticed that their linear diameters also correlate well with the width of their integrated H_α line. As the basis of this study, line profiles have been obtained with a scanning Fabry-Perot interferometer.

The implied correlation between the velocity dispersion in a giant HII region and its size is believed to have fundamental importance for the understanding of the nature and origin of such giant HII regions.

In this note the correlation established in members of the Local group and the M81-NGC 2403 group is applied to a redetermination of the distance to M101.

II. OBSERVATIONS

Line profiles of H_α in the largest HII regions in NGC 2366, 2403, 4236, and 6822 and for NGC 5471 in M101 and NGC 604 in M33 have been recorded with a pressure-scanned Fabry-Perot interferometer (Münch and Taylor 1974) attached to the 60-inch telescope at the Palomar Observatory in October 1975 and April 1976. A 62 arc sec field stop was used with an etalon of 159 km sec^{-1} free spectral range crossed with a 10 Å FWHM (full width at half maximum) interference filter. The counts from a Ga-As photomultiplier, along with the C_3H_8 pressure in the etalon, were recorded at the end of 40 second intervals for the fainter nebulae and 20 seconds for the brighter ones. The minimum peak counts obtained in this fashion were 200. The pressure scanning rate was adjusted to yield approximately 5 km sec^{-1} per channel. The zero point of the radial velocity scale and the instrumental profile were determined each night at least once for every HII region observed, by scanning the H_α line of a Plucker discharge tube. The instrumental profile was found to be well represented by a Gaussian function with a dispersion $\beta_i/\sqrt{2}$ of 6.4 km sec^{-1}.

The results of the observations are summarized in Table 1 which contains the parameters found by fitting the observed profiles with a Gaussian

$$I(V) = I_O e^{-(V-V_O)^2/\beta_O^2}$$

using standard least squares techniques. The peak counts I_o per second over stellar and dark background, the heliocentric radial velocities V_o and the e-folding widths β_o, together with their rms values are given in Table 1. Sample profiles for one of the faintest HII regions observed, NGC 2403-III, and for one of the brighter ones, NGC 6822-III are shown in Figure 1 together with their least squares representation. Typically, two or more line profiles were determined each night and all nebulae were observed on at least two nights. The parameters given in Table 1 represent averages over all profiles. Also included in Table 1 are line width parameters for several extragalactic HII regions measured by Smith and Weedman (1970, 1972). The profiles obtained by these authors for NGC 5471 and NGC 604 are in good agreement with the observations reported here.

Under the assumption that all observed nebulae have a typical kinetic temperature, $T = 10^{4\circ}$ K, the non-thermal component of the line width, the turbulent velocity V_{turb}, has been deconvolved from the data using

$$V_{turb}^2 = \beta_o^2 - \beta_i^2 - \frac{2kT}{m_H} + \beta_{lamp}^2$$

where k is the Boltzmann constant and m_H the mass of the hydrogen atom. The term B_{lamp} represents the intrinsic broadening of the H_a line of the Plucker tube due to the splitting of the fine structure components of the line. The two principal fine structure components of H_a are separated

by 0.141 Å (Meaburn 1970 and references therein) and, assuming that for the comparison lamp they are Gaussian, and of negligible thermal width, the e-folding width β_{lamp} of the composite line is equal to 6.5 km sec^{-1}. The H_α line of the Plucker discharge tube used in the present observations was scanned with a PEPSIOS spectrometer at a resolution of about 2 km sec^{-1} by Dr. J. Trauger. The spectrometer profile, presented in Figure 2, clearly shows the two principal fine structure components with slightly different intensities. The e-folding width of the observed profile, corrected for instrumental broadening, was found to be 0.14 Å, in agreement with the calculated value assuming a negligible thermal component.

The values of V_{turb} in the areas observed photometrically, in Table 1, cover a range from 14 km sec^{-1}, which is about the mean turbulent velocity of galactic HII regions, to a value twice as high.

III. DISCUSSION

The origin of the apparent highly supersonic velocities measured will not be discussed here. It is of importance, nevertheless, to notice that a clear relationship between V_{turb} and the linear diameter of the corresponding HII region seems to exist. The linear diameters $\langle D_C, D_H \rangle$ determined by Sandage and Tammann (1974a), and reproduced in Table 1, have been plotted against V_{turb} in Figure 3. The linear regression line

$$\text{Log}(\langle D_C, D_H \rangle) = (2.27 \pm 0.19) \quad \text{Log}(V_{turb}) - (0.71 \pm 0.26) \ , \quad (1)$$

with $\langle D_C, D_H \rangle$ in parsecs and V_{turb} in km sec^{-1}, obtained by a least squares fit to the objects listed in Table 1 (calibrators), is seen to represent the data very well. The clear correlation between V_{turb} and $\langle D_C, D_H \rangle$ thus established suggests its use to estimate distances of galaxies from measurements of angular diameters of their HII regions.

The distance determination procedure will be illustrated for the case of M101, where angular diameters (Sandage and Tammann 1974b) and velocity dispersions (Smith and Weedman 1970) are available for NGC 5471, 5462, 5455 and 5461. The corresponding data are given in Table 2 together with the linear diameters $\langle D_C, D_H \rangle$ calculated from eq. (1), and the distances resulting from the angular diameters. The mean distance modulus for M101, 28.68±0.39 (rms), obtained from the average distance calculated for the four HII

regions, agrees well with the modulus of 29.1±0.2 obtained by Sandage and Tammann (1974b). It is, however, somewhat lower than the modulus 29.3±0.3 they adopt for M101 on the basis of their results for the various members of the M101 group (Sandage and Tammann 1974b, 1976). Recently, Bottinelli and Gougenheim (1976) have rediscussed the distance to M101 obtaining a modulus of 28.84±0.08 (rms) and suggesting that M101 may not be at the same distance as the other galaxies in its group. If Bottinelli and Gougenheim are correct, the agreement of the modulus determined from the (V_{turb} - Diameter) relation and from other methods is close — beyond expectations.

Clearly, further applications of the (velocity dispersion-diameter) relation to the determination of extragalactic distances require more extensive observations. As a first step, H_α line measurements for HII regions in galaxies in the Virgo cluster, a crucial object for the determination of the Hubble constant (Sandage and Tammann 1976), will be attempted.

It is not possible at present to explain the physical processes which give rise to the high velocity dispersions in giant HII regions. It may be conjectured, however, that such HII regions (hundreds of parsecs across and containing, say, one hundred O-type stars) are aggregates of individual HII regions of typical galactic dimensions (tens of parsecs and ten O-type stars). Each of the individual HII regions

would be expected to move in the rest frame determined by their exciting stars. The net velocity dispersion of the aggregate HII region would then reflect the relative motions of the various groups of imbedded O-stars. In turn, the total number of O-stars presumably depends on the global mass of the neutral gas-dust complex out of which they form, and this mass may ultimately depend on the total mass of the galaxy.

TABLE 1

DATA FOR GIANT HII REGIONS IN GALAXIES
OF THE LOCAL AND M81-NGC 2403 GROUPS

HII Region	Nights Observed	I_O Counts sec^{-1}	V_O[1] km sec^{-1}	β_O km sec^{-1}	V_{turb} km sec^{-1}	$\langle D_C, D_H \rangle$[4] pc
NGC 588	...	...	...	24.2±0.6[2]	19.4	154[5]
595	...	...	...	30.0 1.1[2]	26.2	300
604	2	7.8±0.8	-240.6±1.0	29.5 1.8[1]	25.2	325
	...	...	...	29.3 0.6[2]	25.5	...
NGC 2366-I	2	22.2±1.0	122.0±2.0	28.3±1.3[1]	23.0±1.6	232
NGC 2403-I	4	8.2±0.1	205.0±1.5	30.0±0.7[1]	25.5±0.8	350
II	3	7.1 0.5	120.9 3.9	32.3 0.2[1]	28.0 0.5	257
III	3	7.7 0.5	89.4 4.2	27.4 0.1[1]	22.1 0.5	215
IV	2	4.4 1.0	153.3 7.0	27.1 2.3[1]	21.6 2.5	206[5]
NGC 4236-I	3	4.9±1.0	85.6±1.5	28.9±1.1[1]	23.7±1.5	279
III	2	2.1 1.0	92 5	...	...	200
NGC 6822-I	3	31.6±0.7	60.7±1.8	21.3±0.2[1]	13.8±0.5	89
III	4	23.1 0.7	53.1 0.8	20.8 0.2[1]	13.2 0.5	54
30 Doradus	...	...	269±2[3]	...	25.0[3]	343

REFERENCES:
1. This work
2. Smith and Weedman (1970)
3. Smith and Weedman (1972)
4. Sandage and Tammann (1974a)
5. Sandage, private comunication

TABLE 2

DATA AND RESULTS FOR HII REGIONS IN M101

HII Region	V_O km sec^{-1}	V_{turb} km sec^{-1}	$\langle\theta_C,\theta_H\rangle$ arc-sec	$\langle D_C, D_H\rangle$ parcecs	R_{M101} Mpc
NGC 5471	289±5 [1]	27.3±3.5 [1]	17.9 [4]	352	4.05
	...	27.4±2.5 [2]	...	...	..
NGC 5461	...	28.3±5.0 [2]	16.9 [4]	378	4.62
NGC 5455	...	33.8±3.5 [2]	14.8 [4]	566	7.88
NGC 5462	...	26.9±3.0 [2]	13.3 [3]	337	5.23

$\langle R_{M101}\rangle$ = 5.45±1.0(rms) Mpc.

REFERENCES: 1. This Work
2. Smith and Weedman (1970)
3. Sandage and Tammann (1974a)
4. Sandage and Tammann (1974b)

REFERENCES

Bottinelli, L., and Gougenheim, L. 1976, Astron. and Astrophys., in press.

Meaburn, J. 1970, Nature, 228, 44.

Münch, G., and Taylor, K. 1974, Ap. J. (Letters), 192, L93.

Sandage, A., and Tammann, G. 1974a, Ap. J., 190, 525.

———. 1974b, Ap. J., 194, 223.

———. 1976, preprint.

Smith, M., and Weedman, D. 1970, Ap. J., 161, 33.

———. 1972, Ap. J., 172, 307.

Tully, B., and Fisher, R. 1976, Astron. and Astrophys., in press.

Figure 1

H_α profiles for one of the faintest HII regions observed, NGC 2403-III, and for one of the brightest NGC 6822-III. The solid line represents a Gaussian least squares fit to the data.

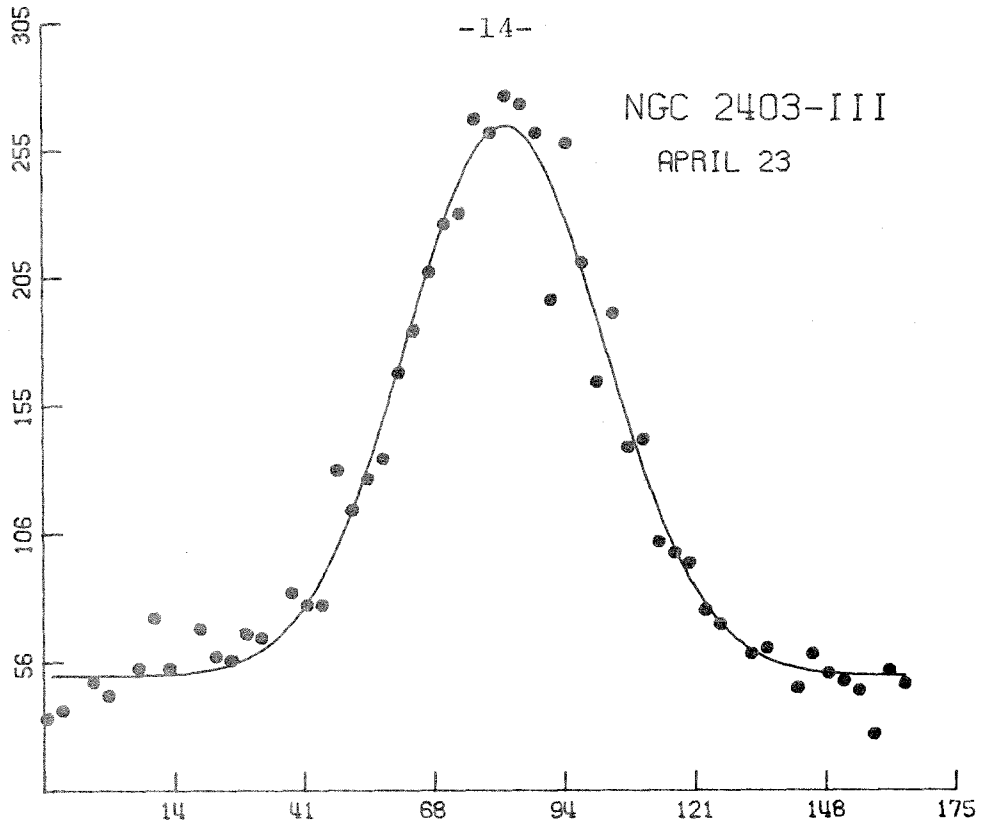
NGC 2403-III
APRIL 23
305
255
205
155
106
56
14
41
68
94
121
148
175

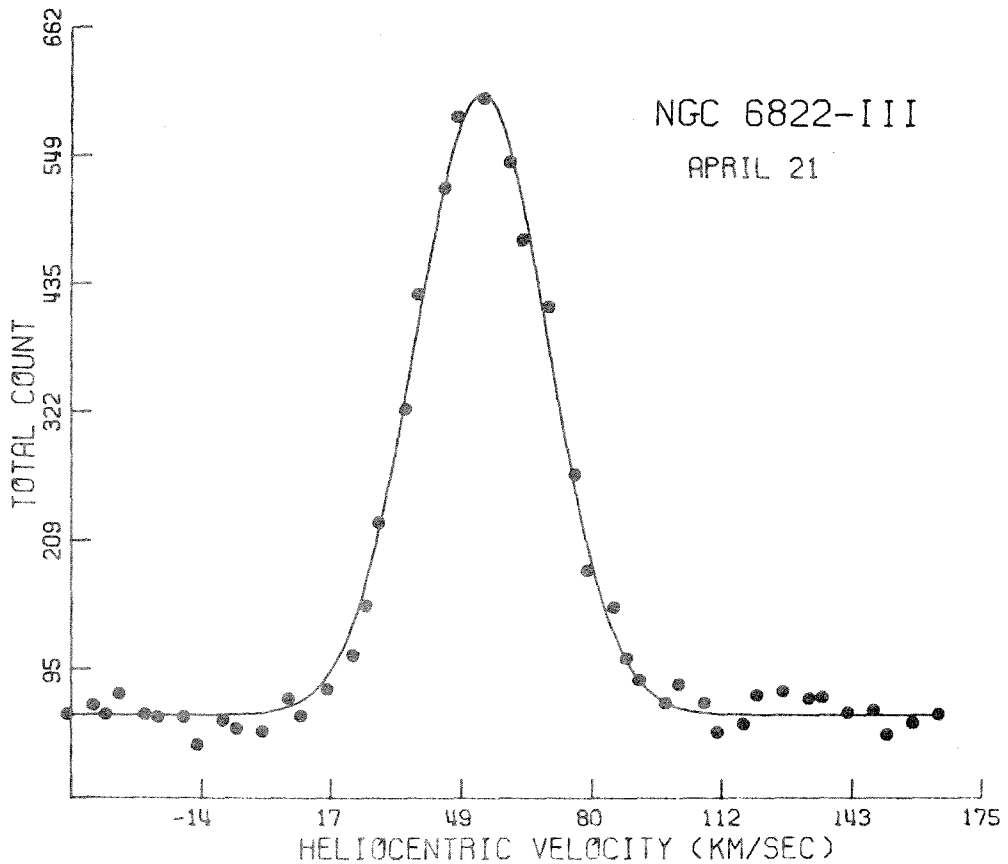
NGC 6822-III
APRIL 21
TOTAL COUNT
662
549
435
322
209
95
-14
17
49
80
112
143
175
HELIOCENTRIC VELOCITY (KM/SEC)

Figure 2

H_α line profile of a Plucker discharge tube. Arbitrary units have been used for the intensities.

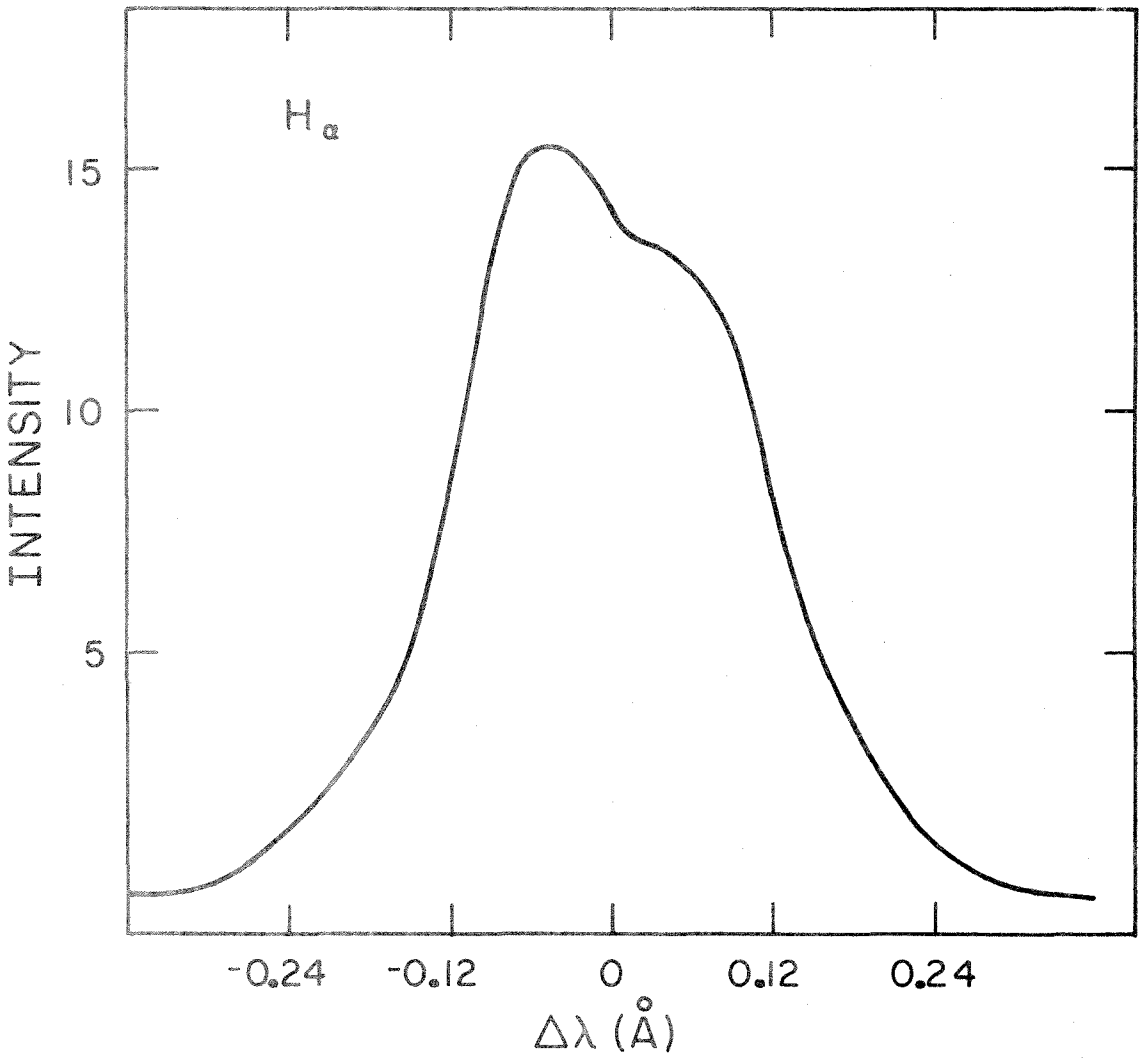
Hα
INTENSITY
15
10
5
-0.24
-0.12
0
0.12
0.24
Δλ (Å)

Figure 3

Plot of Log(V_{turb}) against Log(<D_C,D_H>). The line represents a least squares fit to the data in Table 1. The linear diameters for the HII regions in M101 have been calculated for the distance of 5.45 Mpc to the galaxy derived in the text.

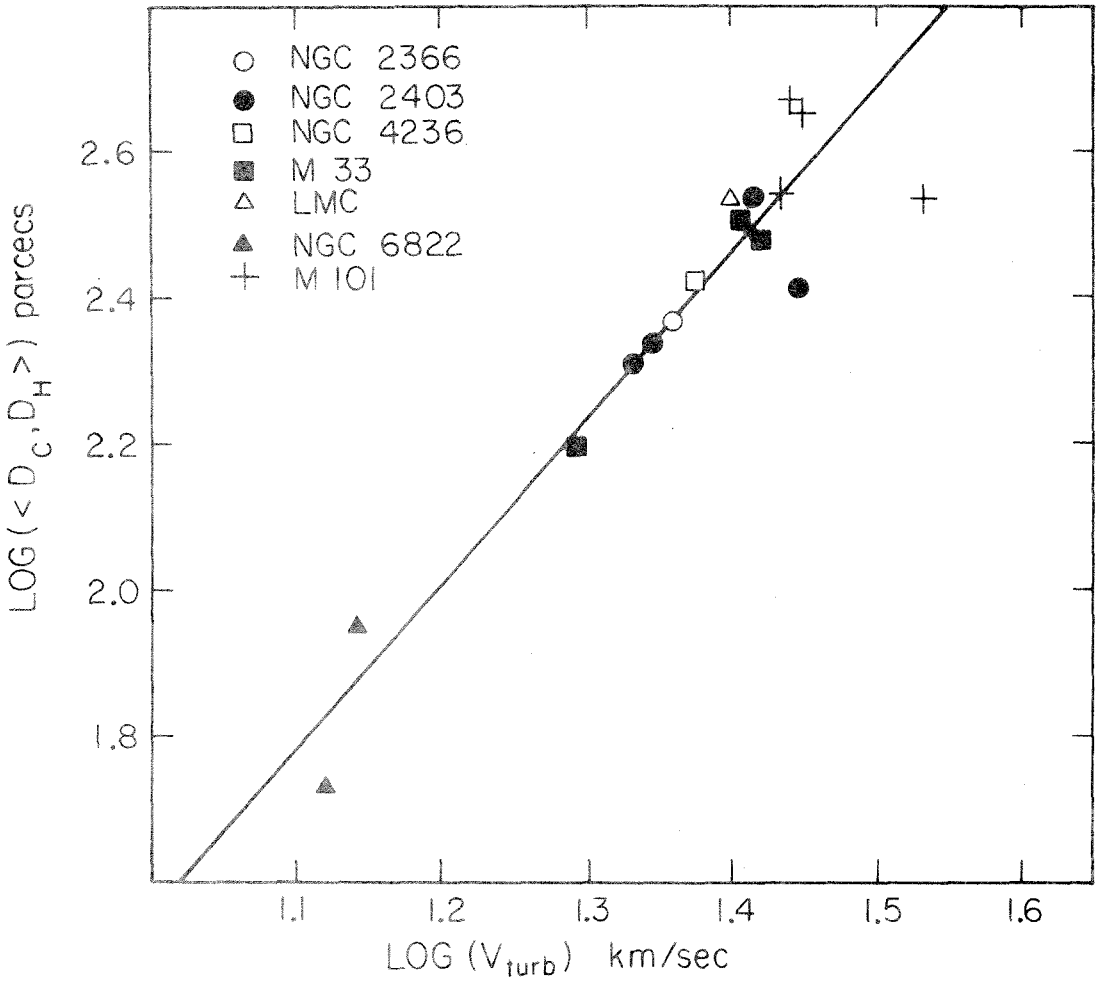
NGC 2366
NGC 2403
NGC 4236
M 33
LMC
NGC 6822
M 101
2.6
2.4
2.2
2.0
1.8
1.1
1.2
1.3
1.4
1.5
1.6
LOG (< D_C, D_H >) parcecs
LOG (V_{turb}) km/sec

PART II

THE (LINEAR DIAMETER — LUMINOSITY) RELATION FOR GIANT EXTRAGALACTIC HII REGIONS

I INTRODUCTION

In a previous Paper (Melnick 1976a, Paper I) an empirical correlation was established between the turbulent component of the integrated H_α line profile widths of giant extragalactic HII regions and their linear diameters as determined by Sandage and Tammann (1974a,b). The correlation, calibrated on members of the Local and NGC 2403 groups, was used to derive a distance of 5.5 Mpc to M101, in good agreement with other determinations (Sandage and Tammann 1974b and 1976; Bottinelli and Gougenheim 1976).

Since the determination of diameters of giant HII regions is somewhat subjective because of the intricate structure presented by these nebulae, and since the observed dimensions depend rather strongly on the plate material used in their determination, further application of the method requires plates and measurement criteria similar to those used by Sandage and Tammann for the calibrators. Clearly, this is not always possible and systematic errors will be introduced if different plates and different definitions of the diameters are used.

Recombination theory, on the other hand, predicts that the Balmer-line flux from a homogeneous dust-free HII region is proportional to its volume. Therefore, if a strong correlation between, say, H_β fluxes and turbulent velocities can be established, it would then be possible to determine

distances to nearby late type spirals from the direct Fabry-Perot observations of their largest HII regions, thus avoiding completely the difficulties involved in the determination of their linear diameters. The method would be particularly useful to determine distances to face-on spiral galaxies for which the 21 cm Tully-Fisher method (Tully and Fisher 1976) cannot be applied.

This Paper reports observations of the integrated H_β fluxes from all HII regions considered in Paper I for which turbulent velocities have been determined.

The characteristics of the dust distribution in the nebulae, which is the factor limiting the application of the $(V_{turb} - I(H_\beta))$ relation to the determination of distances, have been studied in great detail.

II OBSERVATIONS

Most HII regions described in Paper I have angular dimensions which exceed 25 arc-seconds. This implies that simultaneous determination of their integrated absolute H_β fluxes and Balmer decrements is not possible using either the Mount Wilson or Palomar photoelectric spectrum scanners for which the largest available entrance aperture is 25 seconds of arc. Consequently, the H_β fluxes were determined separately using a photometer and interference filters. The two sets of observations are described below.

a) H_β Photometry

The H_β emission fluxes from all HII regions described in Paper I were determined using the Palomar 60-inch telescope with the standard two-channel photoelectric photometer. The Strömgren H_β and 4650 Å interference filters (Crawford 1966) were used to isolate the line emission from the nebula and the contribution to the fluxes in the H_β filter due to the nebular continuum (mostly light from the imbedded stars scattered by dust). All nebulae were observed through apertures at least as large as their halo dimensions as determined by Sandage and Tammann (1974a), and about one-half of them were observed through a series of at least three concentric apertures in order to compare their photometric dimensions with the

sizes determined on photographic plates by Sandage and Tammann.

While the nebulae were being observed in one aperture, the sky and the brightness from the arm of the parent galaxy were simultaneously being observed through the second aperture located 210 seconds of arc away. Each aperture was calibrated and reduced separately and both were then subtracted.

The observations were tied each night to the absolute calibration of α Lyrae (Oke and Schild 1970) through observations of three subdwarf F stars selected from the list of standards for the Hale telescope multichannel spectrophotometer (Oke 1969). One of the stars, HD 19945 was found to have significant H_β absorption and was not used to calibrate the line filter, but the three stars were used to calibrate the continuum channel. Extinction coefficients were determined each night and they showed no significant difference from the mean tabulated values for Palomar. The reductions were carried out using the usual (OB-AB) procedure described by Oke (1965), adopting the bandpasses of the filters as defined on the laboratory. The AB values for the calibration of the continum were defined as

$$AB_{Cont} = \frac{\int C(\lambda) AB(\lambda) d\lambda}{\int C(\lambda) d\lambda}$$

where $C(\lambda)$ is the spectral response of the filter and $AB(\lambda)$ is the monochromatic flux of the standard stars.

Denoting by AB_C and AB_L the continuum and H_β magnitudes of the nebulae, it can be verified that, if the continuum is reasonably flat over the wavelength range covered by the filters (as is shown by the observations of Searle 1971 and Smith 1975), then

$$A \equiv 10^{-0.4\ AB_L} - 10^{-0.4\ AB_C} = \frac{\int L(\lambda) P_\beta(\lambda) d\lambda}{\int L(\lambda) d\lambda} .$$

Here $P_\beta(\lambda)$ is the H_β line profile of the nebula and $L(\lambda)$ the spectral response of the line filter. Laboratory tracings show that on an f/8.75 beam $L(\lambda)$ can be very accurately approximated by a Gaussian function of 63 percent peak transmission I_L at 4861 Å and e-folding width, β_L, of 20 Å. Since the interferometric observations presented in Paper I show that in most nebulae the width of the emission lines is less than 0.6 Å, the absolute H_β fluxes from the HII regions measured outside the earth's atmosphere, $F(H_\beta)$, are to a high degree of approximation given by

$$F(H_\beta) = 4.63 \times 10^{-9}\ (A/I_L)\ e^{\Delta\lambda^2/\beta_L^2} ,$$

where $\Delta\lambda$ is the wavelength shift of the lines due to the overall motion of the nebulae. The resulting $F(H_\beta)$ values are presented in the second column of Table 1.

A conservative estimate for the errors involved in the observations and the reduction procedure is $\pm 0^m.1$. However, possible systematic errors could be somewhat larger for the largest nebulae due to non-uniform illumination of the photocathode.

The results of the multi-aperture observations are presented in Figures 1 and 2. It can be seen in these figures that the photometric and photographic dimensions are in generally good agreement.

b) Spectrophotometry

The H_α, H_β , and [OIII] λ5007 fluxes from the nebulae were determined using the single channel photoelectric spectrum scanner at the Cassegranian focus of the 100-inch telescope at Mount Wilson with 80 Å spectral resolution, and the two-channel scanner with the 60-inch telescope of the Palomar Observatory at a spectral resolution of 66 Å. The largest available field stops of 25 arc-sec at Palomar and 20 arc-sec at Mount Wilson were used.

Each night the observations were tied to the absolute calibration of α Lyrae (Oke and Schild 1970) using the same procedure described above. At least one continuum point adjacent to each emission line was observed and the sky and parent galaxy's arm contributions were subtracted at Mount Wilson by offseting the telescope to a nearby position close to the HII region and at Palomar by using the second aperture, 52 seconds of arc away. The results are presented in Table 1 where column 3 gives the observed H_α to H_β ratios and column 4 the [OIII]/H_β ones.

The logarithmic H_β absorption coefficient $C(H_\beta)$ =

log $I(H_\beta)$ - log $F(H_\beta)$ where $I(H_\beta)$ represents the emitted flux from the nebula, has been calculated assuming that all the reddening takes place outside the nebula from the expression

$$\log \frac{F(H\alpha)}{F(H\beta)} = \log \frac{I(H\alpha)}{I(H\beta)} + C(H_\beta) f(\lambda). \quad (1)$$

The theoretical recombination value $\log\left[I(H_\alpha)/I(H_\beta)\right] = 0.454$ calculated by Blocklehurst (1971) for a case B nebula at 10^4 ^oK has been used together with Peimbert and Torres-Peimbert's (1974) interpolation of Whitford's (1958) extinction law for $f(\lambda)$.

Table 2 summarizes the physical parameters that can be directly derived from the H_β fluxes assuming that eq. (1) applies and that the nebulae are optically thick to radiation shortward of Lyman α. Also included in Table 2 are the linear diameters of the nebulae $\langle D_C, D_H \rangle$ determined by Sandage and Tammann (1974a,b), and the corresponding turbulent velocities taken from Paper I. Column 4 gives the absolute H_β fluxes corrected for absorption by dust using the observed Balmer decrements. In the cases where the observed decrements yielded negative values for the absorption, the corrections determined by Searle (1971) and Smith (1975) were used. For the HII regions in NGC 2366 and NGC 4236, for which no published observations exist, the absorption corrections were determined using the observed H_β fluxes listed in Table 1 and the H_α fluxes

estimated from the Fabry-Perot observations of Paper I, calibrated via the known fluxes of NGC 6822-I and 6822-III. Columns 5 and 6 give the ionizing photon flux required to produce the observed H_β line emission, $S_u(0)$, and the corresponding energy fluxes calculated assuming that the stars radiate like black bodies at a temperature of 55,000° K. The number of O5 stars required to produce those fluxes, N_s, calculated using the model atmospheres computations given by Searle (1971) are presented in 7.

Finally, column 8 gives the ionization parameter $Rn_e^{2/3}$ for a nebula of Strömgren radius R and uniform electron density n_e.

c) Interferometric Observations of NGC 604

Because of its large angular extent and relatively high surface brightness, the giant HII region NGC 604 in M33 was observed interferometrically through a series of concentric apertures ranging from 16" to 78" in diameter. The observations were carried out with the two etalon pressure scanned Fabry-Perot interferometer at the 60-inch telescope at Palomar. The instrument and the observation and data reduction procedures have been described in detail in Paper I.

Two H_α line profiles were obtained through each aperture on two consecutive nights in October 1975. The e-folding widths, V_{turb}, of the observed profiles, deconvolved

from instrumental and thermal broadening, are presented in Figure 2 where V_{turb} has been plotted against aperture diameter in parsecs. The error bars represent rms deviations from the mean of the two profiles determined for each aperture.

The profiles obtained through the largest and smallest apertures are presented in Figure 3 along with their Gaussian least squares representation.

In addition to the concentric aperture observations, the profiles of two 16" spots in the halo of the nebula were obtained. Their average V_{turb} was 17.5 ± 3 km sec^{-1}.

d) Comparison with Radio and Other Optical Observations

The detailed aperture synthesis maps available for M33 and M101 at several continuum wavelengths (Israel 1975 and references therein) can be used in conjunction with the present H_β observations to estimate the net optical depths of the HII regions in these galaxies due to absorption by dust.

In the absence of extinction, the ratio of 21 cm continuum to H_β fluxes is given by

$$\frac{I(21cm)}{I(H_\beta)} = 3.16 \times 10^{-14} \left(\frac{T_e}{10^4}\right)^{0.34} Hz^{-1} \qquad (2)$$

where T_e is the electron temperature of the emitting gas. A comparison between the emitted H_β fluxes, $I(H_\beta)$, derived from Eq. (2), with the observed fluxes of Table 1, leads to the determination of the total H_β absorption, which will be called $A_{rad}(H_\beta)$. The absorption derived from the Balmer decrement and Eq. (1) will be denoted $A_{opt}(H_\beta)$.

Table 3 presents in column 2 the observed 21 cm to H_β flux ratios determined from the radio observations of Israel and Van der Kruit (1974), Israel et al. (1975) and Israel (1975). Column 3 gives $A_{rad}(H_\beta)$ and column 4 presents the values of $A_{opt}(H_\beta)$ derived by Smith (1975) from observations of a small (2" x 2") area in the brightest parts of the nebulae. Column 5 gives $A_{opt}(H_\beta)$ from observations by Searle (1971) plus the present work, both covering in most cases a significant fraction of the total size of the HII regions.

The radio structure of the largest HII regions observed at Westerbork (Israel 1975) has been described in terms of a dense, compact core and a diffuse halo. This kind of structure is immediately apparent on photographs of the 30 Doradus Nebula in the Large Magellanic Cloud (LMC) (Melnick 1976b, Paper III), and can also be clearly seen on more distant nebulae. Figure 4 (Plate 1) presents photographs of the HII regions NGC 604, NGC 2403-II and NGC 5455 in M101, taken with an image tube and a 50 Å wide (FWHM) H_α interference filter. Despite the broad range in distances, the core-halo structure of the three nebulae is apparent.

Table 4 summarizes the optical and radio core-halo parameters derived for NGC 604 using the results presented in Figure 2 and the radio observations of Israel and Van der Kruit (1974). Column 2 presents the core and the halo diameters determined by Israel and Van der Kruit from the apperture synthesis maps of the nebula. Column 3 gives the H_β fluxes for the core and the halo determined from the observations presented in Figure 2 using the radio dimensions of both components, and column 4 lists the corresponding 21 cm fluxes. Columns 5 and 6 present the electron densities determined by Israel and Van der Kruit from the radio observations, and the densities derived from the present H_β results. The H_β absorption in magnitudes $A_{rad}(H_\beta)$ defined above, is listed in column 7. Column 8 gives the turbulent velocities for the core and the halo. The

turbulent velocity for the nebular halo was determined assuming that its H_α line profile can be approximated by a Gaussian function. This is a reasonable assumption since the observations of the overall nebula and of the nebular core are seen in Figure 3 to be well represented by Gaussian distributions.

III RESULTS

a) Core-Halo Structure

The observations presented in Table 4 clearly show that the core and the halo of NGC 604 have very different physical characteristics. The halo shows little or no extinction and very low electron densities. In addition, the observed line width of the halo is significantly smaller than that of the nebular core. Israel (1975) has obtained high resolution radio maps of the nebula at 6 cm which show that the nebular core is formed of at least two and possibly as many as five condensations. This would explain why the nebular H_α line profiles first become wider with increasing aperture size, as more central components are being observed and then, as the halo contribution becomes stronger the profiles become narrower again (cf Figure 2).

In view of this results and the results for the 30 Doradus Nebula presented in Paper III, and following the radio observers, giant extragalactic HII regions will be regarded as composed of a bright, dense core in which most of the ionizing stars and most of the dust are imbedded, and a diffuse halo being ionized by individual stars, not obviously conected with the central cluster which produces the ionization of the core. The complicated network of loops and filaments which appears to characterize the halo

of giant HII regions (cf Figure 4) will be analyzed in detail in Paper III.

b) The Distribution of Dust

The observations presented in Table 3 clearly show that the total absorption at H_β as derived from the 21 cm radio continuum observations are systematically larger than the optical depths derived from the Balmer decrements using Whitford's normal extinction curve. Both the radio and the optical extinctions were determined on the assumption that the absorbing dust is in front of and unmixed with the gas. If this is the case, the observed discrepancy must mean that a different extinction law is followed by the dust near these HII regions. It is easy to see, that, to explain the observed differences, the ratio $R = A_\beta/E(\beta-\alpha)$ between the total extinction at H_β and the $(\beta-\alpha)$ color excess must be in the range $3<R<8$ where 3 is the normal Whitford value. The observations presented in Table 3, however, show that the dust and the gas must be mixed to some extent inside the nebulae; the values of the extinction in the brightest parts of the nebulae as determined from Smith's (1975) observations are systematically larger than the overall absorption as determined from the observations here reported and from those by Searle (1971). A similar correlation between surface brightness and reddening was

been observed in the Orion Nebula (Münch and Persson 1971) and in the 30 Doradus Nebula (Paper III).

In a mixed configuration of dust and gas, the discrepancy between the radio and optically determined extinction is most simply explained if sufficiently large amounts of dust are imbedded in the nebulae. This can be quantitatively seen as follows:

Consider a situation in which dust and gas are well mixed and in which, for simplicity, the albedo of the dust particles at the frequencies of interest here is assumed to be zero†. The radiative transfer equation for this

---

† Münch and Persson (1971) have used the numerical calculations by Mathis (1970) to show that, if the albedo ω is smaller or equal to 0.7, and independent of wavelength for single scattering, this assumption does not change the final results. The situation, however, may be completely different for $\omega = \omega(\lambda) > 0.7$.

---

configuration is simply

$$\frac{dI(\lambda)}{dr} = \varepsilon(\lambda)N_e^2 - N_d\kappa(\lambda)I(\lambda) \qquad (3)$$

where $\varepsilon(\lambda)$ represents the emissivity of the gas for the 21 cm radiation or the recombination coefficients for the Balmer lines. $\kappa(\lambda)$ is the absorption cross section of the dust particles which will be assumed to be proportional to the geometrical cross section of the dust grains σ times a monotonic function of wavelength $f(\lambda)$ representing the reddening

properties of the dust. The solution to eq. (3) is

$$I(\lambda) = \frac{\varepsilon(\lambda)}{\kappa(\lambda)} \int_0^r \frac{N_e^2(r)}{N_d(r)} \exp[-\tau(r)]dr \qquad (4)$$

where $\tau(r) = \int_0^r N_d(x)\kappa(x)dx$.

The observations presented in Table 3 indicate that the H_β absorption $A_{opt}(H_\beta)$ determined from the Balmer decrements tend to a limiting value of nearly $1^m.2$ for large optical depths. This implies that the ratio N_e^2/N_d can increase with optical depth only up to a maximum critical value. Assuming the dust-to-gas ratio to be a constant, eq. (4) can be readily integrated to

$$I(\lambda) = \frac{\varepsilon(\lambda)}{\sigma} \frac{N_e^2}{f(\lambda) N_d} [1-\exp(-\tau_\lambda)] \qquad (5)$$

where now $\tau_\lambda = \kappa(\lambda)N_d R$ for a nebula of radius R. From this equation the ratio between the observed H_α and H_β fluxes is given by

$$\frac{F(\alpha)}{F(\beta)} = \frac{\varepsilon(\alpha)f(\beta)}{\varepsilon(\beta)f(\alpha)} \frac{(1-e^{-\tau_\alpha})}{(1-e^{-\tau_\beta})} \exp(\tau_\beta^{ext}-\tau_\alpha^{ext}). \qquad (6)$$

Since most observed nebulae are at high galactic latitudes and since the observations of NGC 604 show that there is almost no extinction outside the nebula the optical depth due to external dust, τ^{ext} will be ignored. For $\tau \to \infty$ therefore, equation (6) becomes

$$\left.\frac{F(H_\alpha)}{F(H_\beta)}\right|_{lim} = 2.85\ \frac{f(\beta)}{f(\alpha)} \qquad (7)$$

The ratio between the 21 cm radio continuum flux and the H_β luminosity is similarly given by

$$\frac{I(21cm)}{I(H_\beta)} = \frac{\varepsilon(21)}{\varepsilon(\beta)}\ \frac{\tau_\beta}{(1-e^{-\tau_\beta})} \qquad (8)$$

where τ_β is the net optical depth at H_β due to the dust imbedded in the nebulae. From the observed $F(21cm)/F(H_\beta)$ values of Table 3 and the theoretical $\varepsilon(21)/\varepsilon(\beta)$ ratio computed from eq. (2) for $T_e=10^{4\circ}$ K the average optical depths for the HII regions of the three galaxies represented in Table 3 have been derived. The results are presented in Table 5, using the following notation: $E(\tau)= \tau/(1-e^{-\tau})$; N_d= dust density by number calculated from the optical depths using the core sizes of the nebulae R_C and a geometrical cross section of 7×10^{-10} cm^2 estimated by Osterbrock (1974 p.180) for dust grains in galactic HII regions. The gas-to-dust ratio by mass ρ_g/ρ_d has been estimated using the particle densities determined from radio continuum observations (Israel 1975 and references therein) and a mean density of 1 gm cm^{-3} for the dust grains, assuming a pure hydrogen nebula. The last column of Table 5 gives $R_{H\beta}/R_C = 1/\tau_\beta$. This ratio represents the effective depth over which the H_β line formed. The results

of Table 5 confirm that the value $A_{opt}(H_\beta) \sim 1.^m2$, estimated above as the maximum value that can be derived from the Balmer decrements, corresponds to a limiting value for very large optical depths. From eq. (7) and the corresponding limiting value for $F(H_\alpha)/F(H_\beta)$ of approximately 4.0 one finds $f(\beta)/f(\alpha) = 1.40$ significantly different from the value of 1.58 derived by Münch and Persson (1971) for Whitford's extinction law. It is concluded, therefore, that the reddening properties of the dust in giant HII regions are similar to but significantly different from those of the dust found in most places in our Galaxy. It is interesting to note that, using different arguments, Münch and Persson (1971) arrived at the same conclusion for the Orion Nebula. It will be shown in Paper III that the reddening law followed by the dust grains in the 30 Doradus Nebula is identical to that found by Münch and Persson for the nebular light of the Orion Nebula, and by Whiteok (1966) for the light of the stars imbedded in Orion.

Based on the large amounts of dust associated with giant HII regions and on their normal gas-to-dust ratio (Table 5) it might be inferred that these nebulae would be strong inferred sources; yet Strom et al. (1974) report that none of the largest HII regions discussed here are observable at 10 or 20 microns. This clearly indicates most of the dust must not be hot enough to radiate at these wavelengths. On the basis of a rather weak correlation

between 1-25μ infrared luminosity and centimeter radio flux established for galactic HII regions (see for example Wynn-Williams and Becklin 1974; Osterbrock 1974), Strom et al. predict large 10μ infrared fluxes for the extragalactic nebulae. It should be pointed out, however, that the correlation between radio and 1-25μ infrared fluxes has been established for compact HII regions in our Galaxy selected for their strong infrared luminosities. There is no reason to believe that this relation should be valid for nebulae as different as the giant HII regions found in external galaxies. Furthermore, Wynn-Williams and Becklin (see also Osterbrock 1974) have shown that the observed correlation between radio and infrared fluxes implies that absorption of resonantly trapped Lyman α photons can not alone account for the heating of the dust. Part of the heating must therefore be caused by direct absorption of UV photons from the ionizing stars. Only the dust that is very close to the stars can be expected to be hot enough to radiate in the 1-25μ wavelength region.

Table 2 shows that several hundred ionizing stars are required to account for the observed H_β and 21 cm fluxes of the largest nebulae. If each star is assumed to be surrounded by an HII region, say, like the Orion Nebula, a net 10μ infrared flux of less than 10 mfu would be expected for an HII region like NGC 604, well within the limits reported for this nebula by Strom et al. (1974)

c) Distance Determination

It was proposed in Paper I that distances to late type spirals can be determined from the linear diameters of their largest HII regions and the corresponding turbulent velocities. As can be appreciated from Figure 4, the shapes of giant HII regions are often extremely irregular; this means that the determination of their linear dimensions is a very difficult problem. Furthermore, since there are no objective criteria for establishing the boundaries of such HII regions, and since their observed sizes strongly depend on the plate material used in their determination (Sandage and Tammann 1974a), it is in principle not possible to directly apply the calibration of the (V_{turb}-Diameter) relation obtained in Paper I to the determination of distances to spiral galaxies. On the other hand, the determination of turbulent velocities and Balmer line intensities is a completely objective observational problem. Thus, the existance of a narrow correlation between, say, H_β fluxes and turbulent velocities in giant HII regions would provide a powerful method for distance determination

Figure 5 presents plots of the H_β intensities of Table 2 against both turbulent velocities and linear diameters. Also shown in that figure are least squares fits to the data with parameters

$$\log I(H_\beta) = (4.2\pm1.2)\log V_{turb} + (33.3\pm1.6)$$

and

$$\log I(H_\beta) = (1.7\pm0.4)\log\langle D_C, D_H\rangle + (35.0\pm0.4)$$

appropriate to a distance of 5.5 Mpc to M101 (Paper 1). The root mean square deviation from the regression lines was found in both cases to be close to 0.5 in $\log I(H_\beta)$ or 1.25 magnitudes.

No significant differences were found in either the fit parameters or the standard errors when the distance of 7.2 Mpc to M101 derived by Sandage and Tammann (1974b) was used (cf Figure 5).

The correlations are seen in both cases to be rather strong. They are, however, flatter than the relations $I(H_\beta) \propto R^3$ and $I(H_\beta) \propto V_{turb}^6$ expected for dust-free homogeneous nebulae. Clearly, the large dispersion observed precludes the application of either relation to the determination of distances. From the discussion presented in the preceding section, it becomes apparent that, to a large extent, the scatter in $I(H_\beta)$ must arise from the uncertainties involved in the reddening corrections. This suggests that in principle it may be possible to establish a close correlation between the 21 cm radio continuum fluxes and the turbulent velocities. Since the radio continuum fluxes are virtually unaffected by dust, the scatter in the (I(21cm) - Diameter) relation must arise only from intrinsic differences in the gas distribution of the nebulae. Figure 6 shows plots

identical to those presented in Figure 5 using the 21 cm fluxes instead of $I(H_\beta)$. The solid lines in this case represent eye fits to the data. It can be seen that the scatter is now significantly smaller than that of the relations for $I(H_\beta)$. However, only half of the nebulae have been plotted in Figure 6. Clearly, more 21 cm observations are required to determine if the (I(21 cm) - V_{turb}) correlation can be applied to the determination of distances to spiral and irregular galaxies.

IV CONCLUSIONS

Possible models for the origin of the supersonic motions observed in giant HII regions will be presented in Paper III. The observations reported here can be used to put constraints on the possible sources of energy for the mass motions. It has generally been proposed (Oort and Spitzer 1955; Münch 1958; Spitzer 1968) that the ionizing radiation from the stars can accelerate the gas through the interaction of ionization fronts with the surrounding neutral material. A lower limit for the ages of the nebulae included in Table 2 can be obtained by requiring that the energy radiated by the exciting stars be converted into kinetic energy by the Oort-Spitzer mechanism. Assuming an efficiency of 0.006 for the conversion (Spitzer 1968), minimum ages of $5X10^5$ years are derived using the physical parameters of Table 2. This is close to the main sequence life of $3X10^6$ years for the exciting stars. Since a significant fraction of the stellar radiation is absorbed by dust as well as radiated away, at least two generations of star formation would be required to produce the motions observed if the motions do not decay. Even then, it is not clear from the numerical calculations (Lasker 1966) that it is possible to account for the highly supersonic velocities of the gas on the basis of the Oort-Spitzer acceleration mechanism. Moreover, if the stellar radiation is

responsible for the supersonic motions observed, the turbulent velocities should be proportional to the ionizing flux density of the stars per unit volume. Figure 8 shows a plot of the ratio $S_u(0)/R^3$ against V_{turb}. The ionizing fluxes derived from both the radio and the optical observations have been used with the core and overall radii of the nebulae as determined by Sandage and Tammann (1974a,b). No apparent correlation can be seen between the specific fluxes and the turbulent velocities.

V SUMMARY

The main conclusions of this Paper are summarized as follows:

1) There are large amounts of dust imbedded in giant extragalactic HII regions; the dust to-gas-ratios are found to be similar to the ratios found in galactic HII regions. As a concequence, the observed Balmer line intensities and colors tend to a limiting value for large optical depths. The reddening law of the dust grains is found to be similar to, but significantly different from Whitford's normal extinction law.

2) A strong correlation is found between the absolute H_β fluxes and the turbulent velocities of the nebulae. The large uncertainties in the extinction corrections, however, preclude the application of this relation in determining distances to galaxies. It is proposed instead, that the correlation between radio continuum fluxes and turbulent velocities may provide a good method for distance determination, since the radio fluxes are not affected by dust.

3) The highly supersonic motions observed in giant HII regions have not been produced by the ionizing radiation of the imbedded stars.

TABLE 1

PHOTOMETRIC RESULTS

HII REGION	$-\log F(H_\beta)$	$\log H_\alpha/H_\beta$	$\log[OIII]/H_\beta$	$C(H_\beta)$
NGC 604	11.15	0.46	...	0.03
595	11.74	0.45	0.17	...
588	12.09	0.54	0.72	0.26
131	12.25	0.42	0.29	...
NGC 2403-I	11.91	0.53	0.29	0.24
II	11.92	0.60	0.11	0.45
III	11.79	0.51	0.21	0.18
IV	12.11	0.48	0.22	0.10
NGC 2366-I	11.72	...	0.86	0.30[1]
NGC 4236-I	12.49	...	0.66	0.27[1]
NGC 6822-I	12.09	0.43	0.60	...
III	12.05	0.52	0.66	0.21
NGC 5471	11.97	0.44	0.87	...
5462	12.37	0.58	0.47	0.39
5455	12.27	0.46	0.10	0.03
5461	11.89	0.49	...	0.12

Notes: [1] Estimated from the Fabry-Perot observations of Melnick (1976a Paper I)

TABLE 2

PHYSICAL PARAMETERS

HII Region	$\langle D_C, D_H \rangle$ (pc)	V_{turb} (km sec^{-1})	$I(H_\beta)$ (10^{38} ergs s^{-1})	$S_u(0)$ (10^{51} s^{-1})	$E_u(0)$ (10^{40} ergs/sec)	N_s	$Rn_e^{2/3}$ (pc cm^{-3})
NGC 588	154	19.4	1.2†	0.2	0.7	7	184
595	300	26.2	4.5††	0.9	3.2	35	324
604	325	25.2	6.9	1.5	5.2	54	356
IC 131	...	21.9	0.6	0.1	0.1	4	162
NGC 2366-I	232	23.0	48.0	10.1	35.5	360	680
NGC 2403-I	350	25.5	27.0	5.7	20.0	205	556
II	257	28.0	42.8	9.0	38.9	324	648
III	215	22.1	38.2	8.1	15.0	292	648
IV	206	21.6	12.3	3.2	11.2	50	453
NGC 4236-I	279	23.7	7.6	1.6	26.6	58	356
NGC 5455	350	33.8	29.0	6.1	21.4	220	183
5461	446	28.3	85.8	18.1	63.4	652	642
5462	391	26.9	53.0††	11.2	40.0	403	745
5471	472	27.3	54.2	11.4	40.0	400	712
NGC 6822-I	89	13.8	2.9†	0.6	2.2	22	292
III	54	13.2	2.0	0.4	1.4	14	227

† $A(H_\beta)$ taken from Smith (1975)

†† $A(H_\beta)$ taken from Searle (1971)

TABLE 3

DUST DISTRIBUTION: COMPARISON
BETWEEN OPTICAL AND RADIO CONTINUUM RESULTS

HII REGION	$-\text{LOG}\frac{F(21cm)}{F(H_\beta)}$	$A(H_\beta)$ RADIO	(1) $A(H_\beta)$ OPT	(2) $A(H_\beta)$ OPT
NGC 604	13.09[1]	$1^m.03$	$0^m.0$[4]	0.22[5]
595	12.96[1]	1.35	1.23[4]	...
588	13.19[1]	0.79	0.75[4]	...
IC 131	13.41[1]	0.23	0.31[4]	0.08
NGC 5471	12.95[2]	1.37	0.51[4]	0.09[5]
5462	12.55[2]	2.37	1.21[4]	0.98
5461	12.83[2]	1.67	1.02[4]	0.30
5455	12.99[2]	1.28	1.18[4]	0.08
NGC 2403-I	12.64[3]	2.16	1.20[4]	0.60

LEGEND: 1 Israel and Van der Kruit 1974
2 Israel et al. 1975
3 Israel 1975
4 Smith 1975
5 Searle 1971

TABLE 4

CORE-HALO PARAMETERS FOR NGC 604

	D pc	$F(H_\beta)$ 10^{38} ergs s^{-1}	F(21cm)† 10^{25} ergs s^{-1}	n_e (cm^{-3}) radio	n_e (cm^{-3}) optical	$A(H_\beta)$ Radio	V_{turb} km sec^{-1}
Core:	42	1.8	3.4	45	36	$1^m.9$	26.8
Halo:	325	3.9	1.2	1	2	0	22.1

†From Israel and Van der Kruit 1974

TABLE 5

THE DISTRIBUTION OF DUST IN GIANT HII REGIONS

Galaxy	$\langle E(\tau) \rangle$	$\langle \tau_\beta \rangle$	$\langle R_C \rangle$	$\langle \log N_d \rangle$	$\langle \rho_g/\rho_d \rangle$	$\langle R_{H\beta}/R_C \rangle$
M33	0.46	2.3	70	-10.8	2600	0.4
M101	0.27	3.6	95	-10.7	1500	0.3
NGC 2403-I	0.14	6.5	84	-10.5	1100	0.2

REFERENCES

Blocklehurst, M. 1971, M.N.R.A.S., 153, 471.

Bottinelli, L., and Gougenheim, L. 1976, Astron. and Astrophys., in press.

Crawford, D. L. 1966, A. J., 71, 114.

Israel, F. P., and van der Kruit, P. C. 1974, Astron. and Astrophys., 32, 363.

Israel, F. P., Goss, W. M., and Allen, R. J. 1975, Astron. and Astrophys., 40, 421.

Israel, F. P. 1975, Mittelberg Conference on H II Regions and Related Topics, eds. T. L. Wilson and D. Downes (Heidelberg: Springer-Verlag), p. 288.

Lasker, B. M. 1966, Ap. J., 143, 700.

Mathis, J. 1970, Ap. J., 159, 263.

Melnick, J. 1976a, Ap. J., Paper I, in press

Melnick, J. 1976b, Paper III, preprint.

Morton, D. C. 1967, Ap. J., 150, 535.

Münch, G. 1958, Revs. Mod. Phys., 30, 1035.

Münch, G., and Persson, S. 1971, Ap. J., 165, 241.

Oke, J. B. 1965, Ann. Revs. Astron. and Astrophys., Vol. 3.

_____. 1969, Pub. A.S.P., 81, 11.

Oke, J. B., and Schild, R. E. 1970, Ap. J., 161, 1015.

Oort, J. H., and Spitzer, L. 1955, Ap. J., 121, 6.

REFERENCES (CONT'D)

Osterbrock, D. 1974, Astrophysics of Gaseous Nebulae (San Francisco: Freeman).

Peimbert, M., and Torres-Peimbert, S. 1974, Ap. J., 193, 327.

Sandage, A., and Tammann, G. 1974a, Ap. J., 190, 525.

_____. 1974b. Ap. J., 194, 223.

_____. 1976, Ap. J., in press.

Searle, L. 1971, Ap. J., 168, 327.

Smith, H. F. 1975, Ap. J., 199, 591.

Spitzer, L. 1968, Diffuse Matter on Space (New York: Interscience Publishers).

Strom, S., Strom, K., Grasdalen, G., and Capps, R. 1974, Ap. J. (Letters), 193, L7.

Tully, B., and Fisher, R. 1976, Astron. and Astrophys., in press.

Whiteoak, J. B. 1966, Ap. J., 144, 305.

Whitford, A. E. 1958, A. J., 63, 201.

Wynn-Williams, G. C., and Becklin, E. E. 1974, Pub. A.S.P., 86, 509.

Figure 1

Multi-aperture observations of eleven giant HII regions in five different galaxies. An arbitrary normalization has been used for the H_β magnitudes, and the aperture diameters are given in seconds of arc.

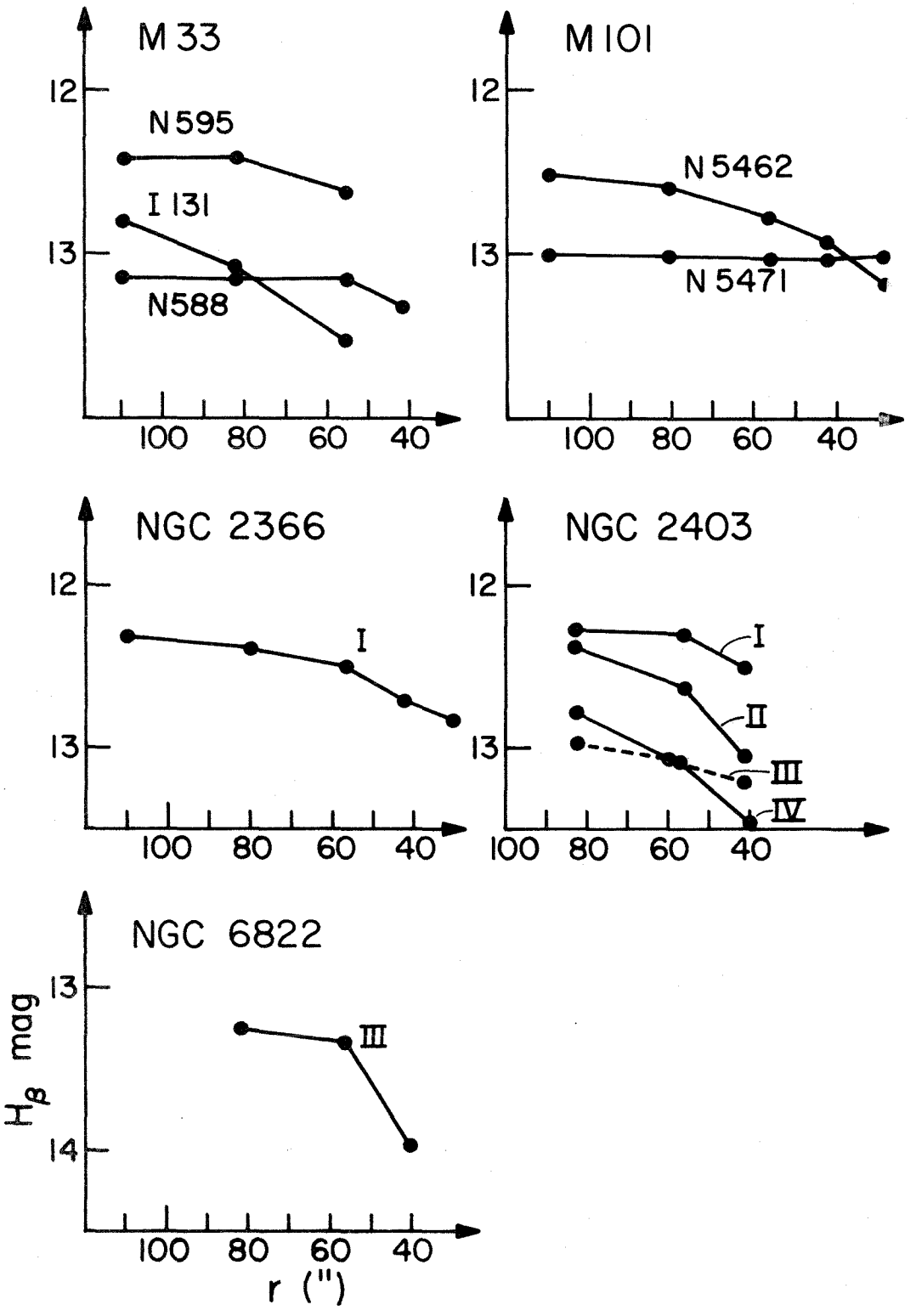
M 33
N595
I 131
N588
M 101
N 5462
N 5471
NGC 2366
I
NGC 2403
I
II
III
IV
NGC 6822
III
12
13
14
100
80
60
40
H_β mag
r (")

Figure 2

Photometric and interferometric observations of the giant HII region NGC 604 in M33 through a series of concentric entrance apertures. An arbitrary normalization has been used for the H_β magnitudes. The flux given in the text for the overall nebula corresponds to 10.9 magnitudes in these units.

The profile widths through each aperture are presented in terms of the turbulent velocity, V_{turb}, defined in the text.

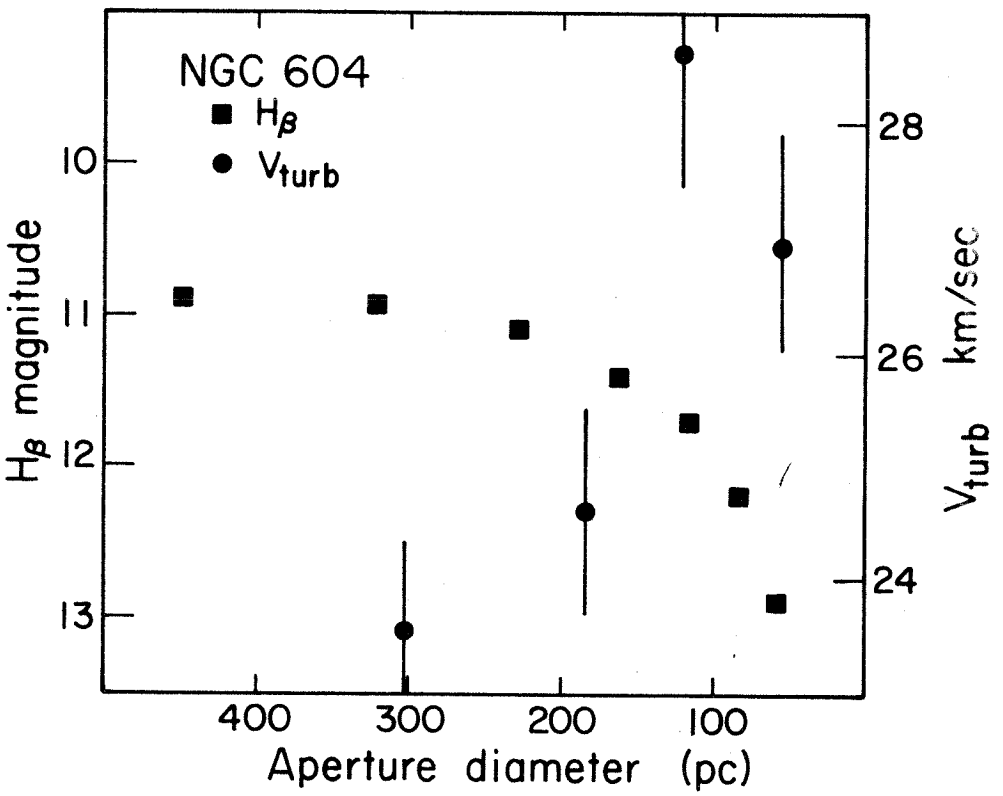
NGC 604
■ Hβ
● Vturb
10
11
12
13
Hβ magnitude
28
26
24
Vturb km/sec
400
300
200
100
Aperture diameter (pc)

Figure 3

Hα line profiles of NGC 604 taken through the 78 arc-sec (top) and the 16 arc-sec field stops. The solid lines represent Gaussian least squares fits to the data.

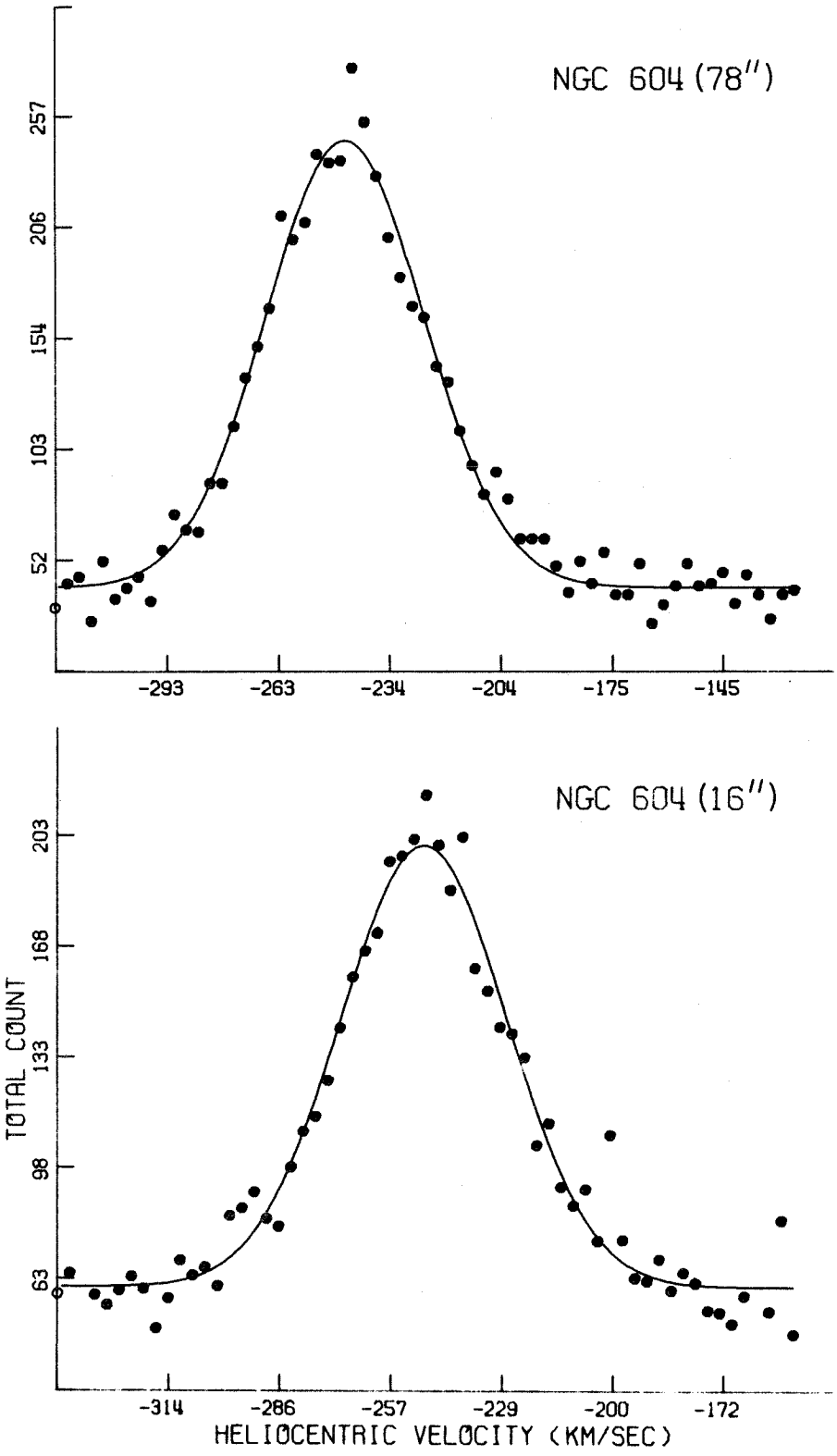
NGC 604 (78″)
257
206
154
103
52
0
-293
-263
-234
-204
-175
-145
NGC 604 (16″)
203
168
133
98
63
0
TOTAL COUNT
-314
-286
-257
-229
-200
-172
HELIOCENTRIC VELOCITY (KM/SEC)

Figure 4

H_α plates of giant HII regions in M33 (R=817 kpc), NGC 2403 (R=3.3 Mpc) and M101 (R=5.5 Mpc). The plates were exposed for 60 minutes (NGC 604) and 45 minutes (NGC 2403 and 5455) on IIa-D emulsion using a 90mm magnetically focused image intensifier at the Palomar 60-inch telescope. A 50 Å FWHM interference filter was used to isolate the H_α line from the nebulae.

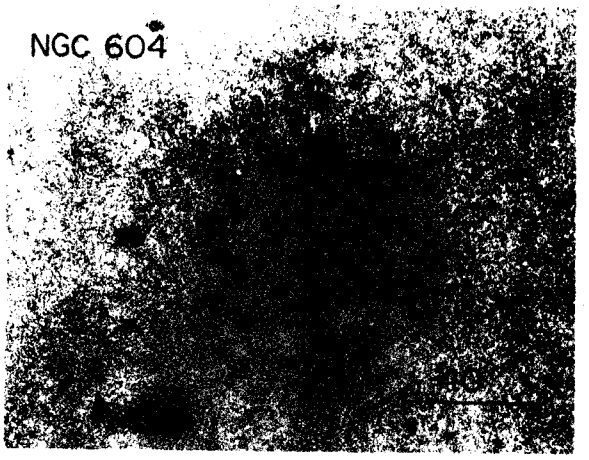
NGC 604

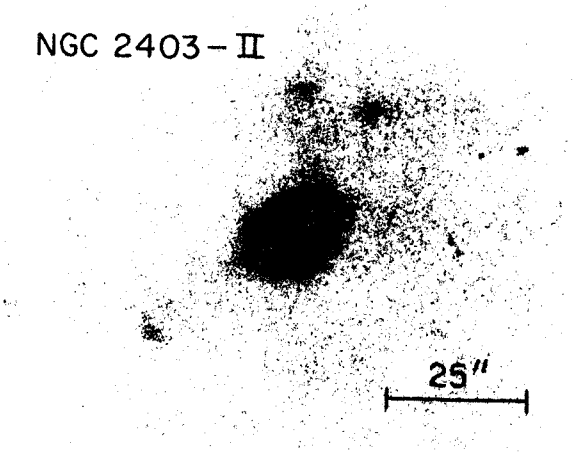
NGC 2403 – II
25"

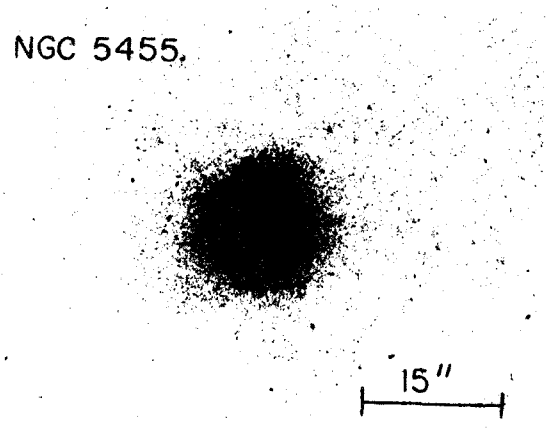
NGC 5455.
15"

Figure 5

Logarithmic plots of the absolute H_β fluxes of the observed HII regions against turbulent velocities (left) and linear diameters (right). The solid lines represent least squares fits to the data. The distances of 5.5 Mpc (paper I) and 7.2 Mpc (Sandage and Tammann 1976) to M101 have been represented on the left plot. The distance of 5.5 Mpc was used in the least squares fit. The LMC point represents the 30 Doradus nebula and the relevant data was taken from Paper III.

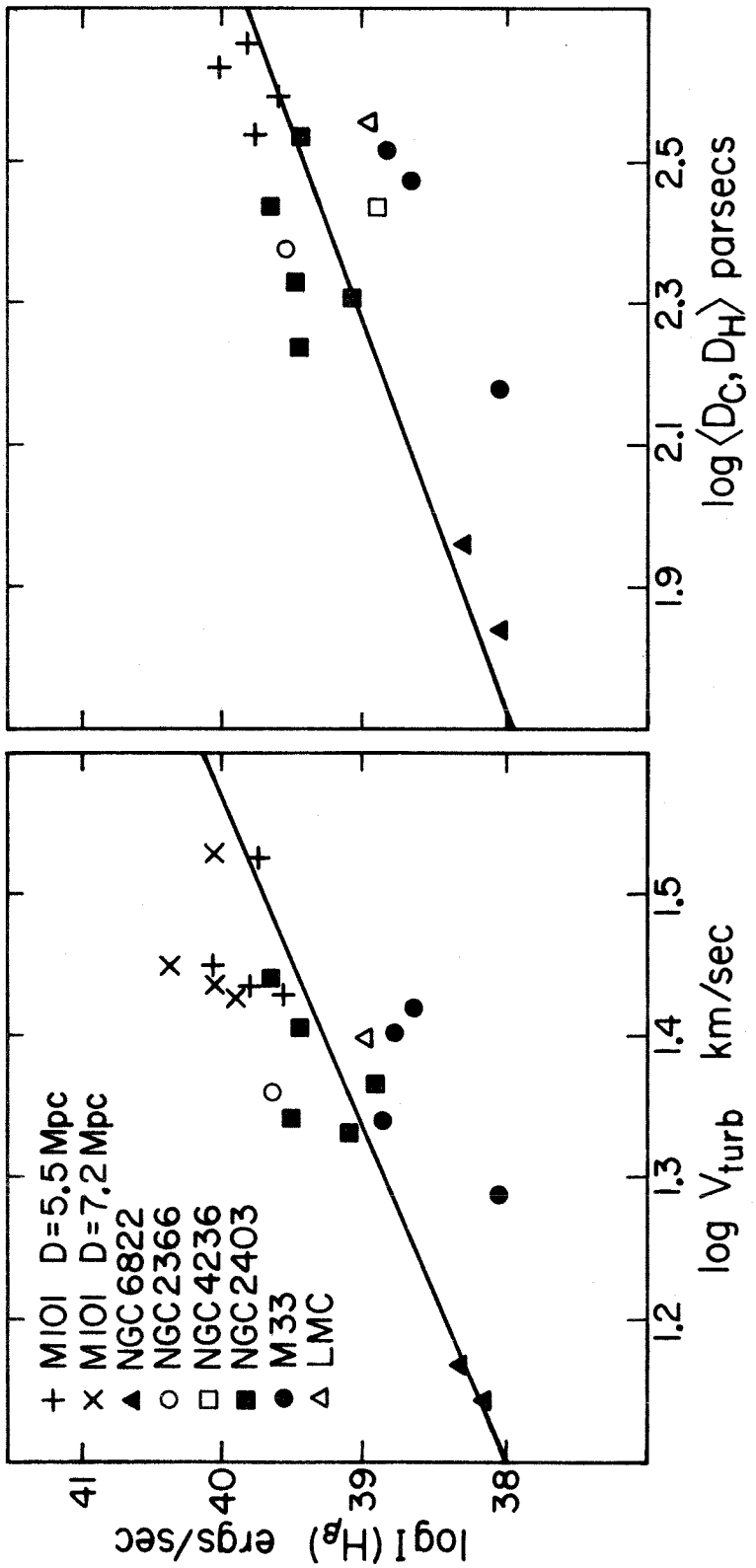
log I (H_β) ergs/sec
41
40
39
38
+ M101 D=5.5 Mpc
× M101 D=7.2 Mpc
▲ NGC 6822
○ NGC 2366
□ NGC 4236
■ NGC 2403
● M33
△ LMC
1.2
1.3
1.4
1.5
log V_{turb} km/sec
1.9
2.1
2.3
2.5
log ⟨D_C, D_H⟩ parsecs

Figure 6

Similar plots to the ones presented in Figure 5 in which the H_β fluxes have been replaced by the 21 cm radio continuum luminosities. The solid lines are eye fits through the data.

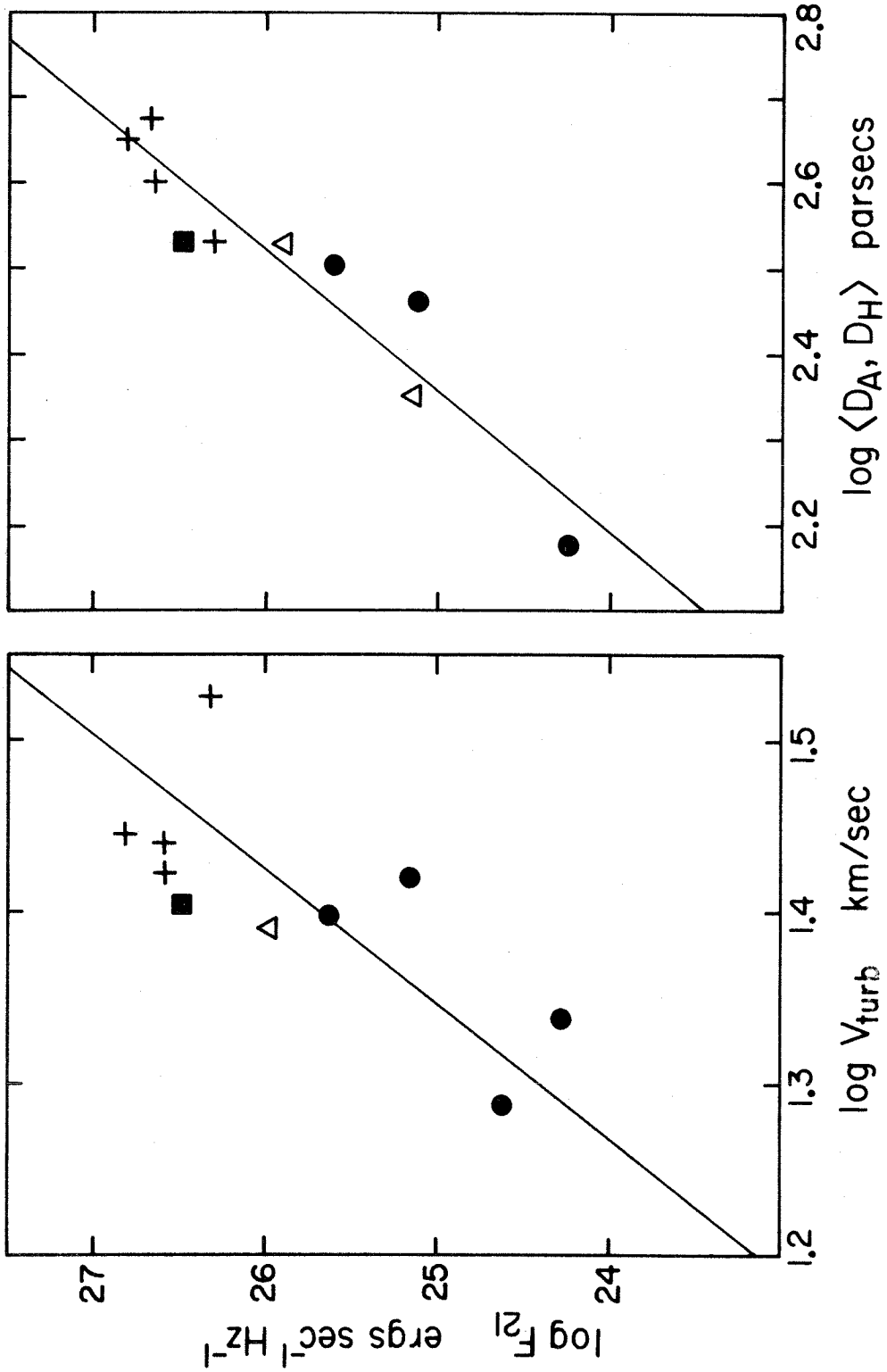
log F_{21} ergs sec^{-1} Hz^{-1}
27
26
25
24
log V_{turb} km/sec
1.2
1.3
1.4
1.5
log $\langle D_A, D_H \rangle$ parsecs
2.2
2.4
2.6
2.8

Figure 7

Logarithmic plots of the ionizing flux per unit volume against turbulent velocity. The optically derived ionizing fluxes (left) and the radio derived ones (right) have been used with the volumes determined from the core (dots) and the overall (crosses) dimensions.

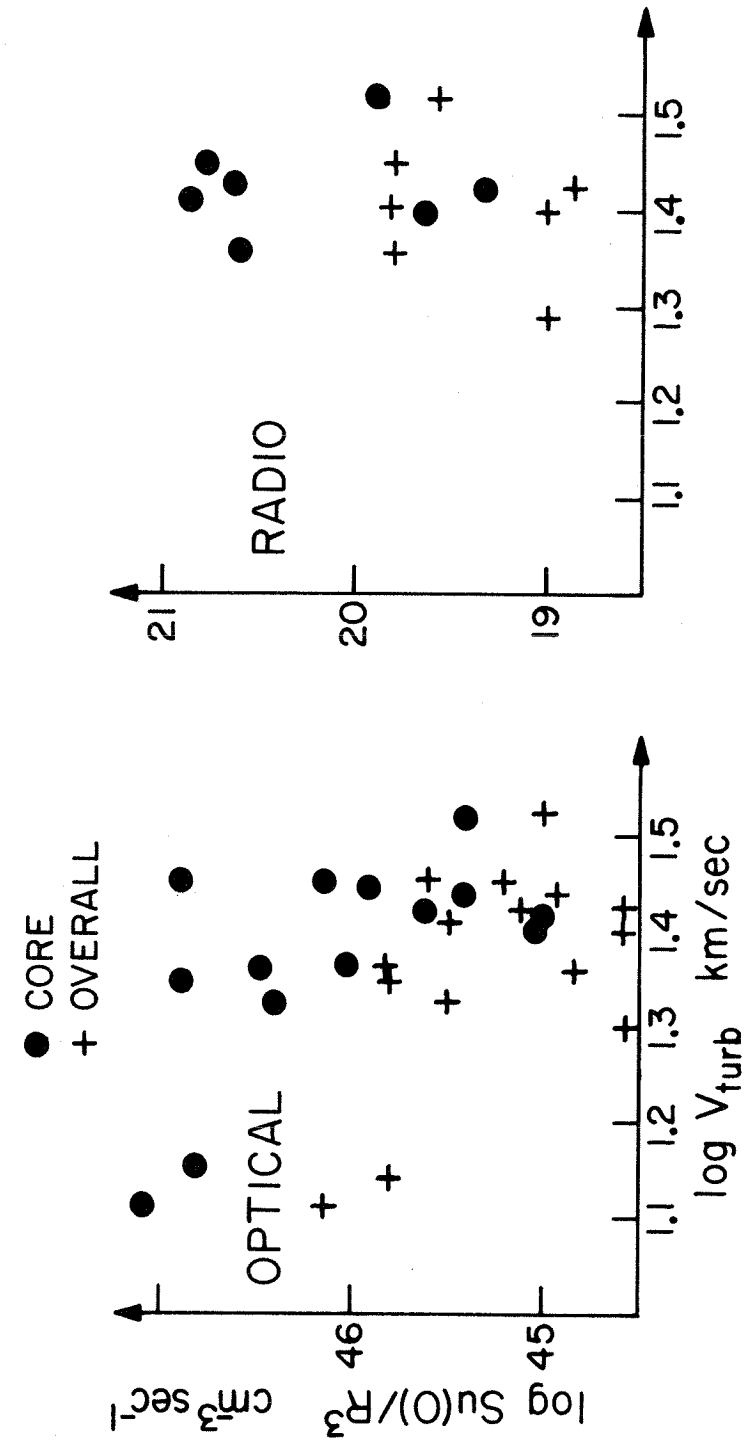
RADIO
OPTICAL
● CORE
+ OVERALL
log Su(0)/R³ cm⁻³ sec⁻¹
log V_turb km/sec
21
20
19
46
45
1.1
1.2
1.3
1.4
1.5

PART III

THE STRUCTURE OF THE 30 DORADUS NEBULA

I INTRODUCTION

The 30 Doradus nebula (NGC 2070) in the Large Magellanic Cloud (LMC), because of its proximity and its angular extent of more than 15 arc-minutes, provides us with a unique opportunity for a detailed study of a giant extragalactic HII region.

The intricate filaments and loops that appear to characterize the halos of giant HII regions (Melnick 1976b, Paper II) are very prominent in 30 Doradus and have led to the names of "great looped" nebula or "tarantula" nebula.

A number of extensive studies of the nebula have been carried out in past years; Feast, Thackeray and Wesselink (1960) and Feast (1961) have studied the brightest stars in the nebula and have concluded that 30 Doradus contains the largest concentration of Wolf-Rayet (WR) stars in the LMC. Westerlund and Smith (1964) have suggested that the WR stars in 30 Doradus are more luminous than the field WR stars in the LMC. Westerlund (1964) has studied the central star cluster of the nebula and has estimated its total stellar mass in 2×10^4 $M_\odot$.

Several spectroscopic studies of the nebula have been undertaken with the aim of determining its physical conditions. In general, temperatures close to 10^4 °K

and mean electron densities of the order of a few hundred cm^{-3} (Feast 1961; Faulkner and Aller 1964) have thus been obtained. The total mass of ionized gas has been estimated by Faulkner (1967) to be of the order of $5 \times 10^5 M_\odot$.

On the basis of a 21 cm radio continuum study for the 30 Doradus Nebula, Mathewson and Healey (1964) proposed the core-halo model currently used to interpret radio continuum observations of giant extragalactic HII regions (Israel 1975). Mathewson and Healey and Le Marne (1968) have indicated that a non-thermal radio source may be associated with the halo of 30 Doradus, but this suggestion has not been confirmed by an identification of such a source.

Faulkner (1967) and Le Marne (1968) have analyzed the reddening properties of the dust near the 30 Doradus Nebula on the basis of a comparison between optical and radio observations and have concluded that the observations could be explained if the absorbing dust was located in front of the nebula and the ratio $R=A_V/E(B-V)$ between the total and the selective absorption was equal to 7.

The dynamics of the nebula has been studied in detail by Feast (1961) and Faulkner (1967) who have concluded that the nebula is gravitationally unbound. By far the most ex-extensive study of the kinematics of the 30 Doradus Nebula, however, have been made by Smith and Weedman (1972). These authors have obtained 200 emission line profiles at

different positions in the nebula using a pressure scanned Fabry-Perot interferometer with a spectral resolution of 11 km sec^{-1}. Smith and Weedman conclude that the most probable turbulent velocity, V_{turb}, in 30 Doradus is about 25 km sec^{-1}, significantly larger than the value of 16 km sec^{-1} found by Feast (1961) from radial velocities alone. On the assumption that the motions in the nebula follow a Gaussian distribution, the most probable velocity is defined as the e-folding width of the velocity profile. Consequently, the most probable velocity is related to the dispersion of the radial velocity profile σ_1 as $V_{turb} = \sqrt{2}\sigma_1$. The three-dimensional velocity dispersion is $\sigma_{turb} = \sqrt{3}\sigma_1$.

The width of the H109α recombination line profiles of the nebula at 5.99 cm (Mezger et al. 1970; Huchtmeier and Churchwell 1974; McGee et al. 1974) indicate turbulent velocities even larger than the ones derived from the optical recombination lines.

In this Paper, the following three aspects of the structure of 30 Doradus will be considered:

1) The core-halo structure. It will be shown that the distribution of ionized gas in the nebular halo closely follows the distribution of individual stars imbedded in it. The gigantic loops of the "great looped" nebula are inter-

preted as being circumstellar shells produced by strong stellar winds. The long, thin filaments which form the "arms" of the "tarantula" appear to be produced by radial magnetic fields (cf Mathewson and Ford 1970).

2) The reddening law of the nebular light. On the basis of spectrophotometric observation at 43 different positions in the nebula, the dust distribution and the reddening law of the grains will be established. It is shown that large amounts of dust must be mixed with the gas within the nebula.

3) The dynamics of the nebular core. It will be shown in this Paper that the core and the halo have very different kinematical properties. The dynamics of the nebular core will be analyzed in terms of a model in which the core is formed by a "cluster" of individual HII regions around individual stars. In the model, the highly supersonic motions observed are interpreted as due to the motions of the individual stars in the aggregate nebula.

II. OBSERVATIONS

a) Spectrophotometry

The intensities of the H_α, H_β and H_γ emission lines at a number of positions in 30 Doradus were measured on the 36-inch telescope at Cerro Tololo Interamerican Observatory in December 1974 and January 1975. The measurements were done using the two-channel Harvard scanner equipped with two cooled FW130 photomultipliers. Forty-three positions in the nebula were observed through 65 arc sec diameter entrance diaphragms, at a spectral resolution of 40 Å in the second order. In addition, fifteen of these positions were also observed at a second order resolution of 20 Å using entrance diaphragms 32".5 in diameter.

During the observations, the entrance apertures, separated by 155", were oriented along the EW or the NS directions. In this way it was possible, to a large extent, to avoid overlapping between different settings on the nebula.

The continuum contribution to the line fluxes, mostly due to stellar radiation scattered by dust, was determined by measuring one continuum point at each side of the observed emission lines. The integration times required to obtain at least two percent statistics over the continuum level were often as long as 30 minutes for H_γ and H_β, but were considerably lower for H_α. To avoid uncertainties due to changes in the sky brightness and possible drifts in the

instrumental characteristics during the integrations, 30-second steps were used for each wavelength setting. The computer-controlled scanner was instructed to automatically chop between the lines and the continuum after each 30-second integration, and it was manually stopped when the required number of counts was reached. Since the Tololo sky is free of strong emission lines in the wavelength region considered by the present observations, it was only necessary to monitor the sky brightness periodically between settings. This was done alternately at four positions: north, south, east and west of the nebula.

The 36-inch telescope is equipped with an offset guider which was used to accurately position the telescope at the desired places on the nebula. This was done by offsetting the two bright stars marked S1 and S2 on Figure 1. The same stars were used to guide the telescope during the integrations. The positioning and guiding errors, determined mostly by the seeing conditions, are estimated to be about 4 arc seconds.

Each night the observations were tied to the absolute calibration of α Lyrae (Oke and Schild 1970) by observing at least three stars from the standard list of Oke (1960), using the tabulated mean extinction coefficients for Tololo. Each channel was calibrated independently.

The calibrations were carried out at the same wavelength points used in the nebular continuum measurements.

The transformation constants (OB-AB) (Oke 1965) at the Balmer line wavelengths were determined by interpolating between the two corresponding continuum calibrations. In this way, it was possible to avoid the strong Balmer absorption lines in the spectrum of some of the standard stars, and, at the same time, minimize the effects of possible non-linearities in the spectral response of the instrument.

The results are presented in Table 1 for the 65" observations, and in Table 2 for the 32".5 observations. Column 1 of Table 1 gives the spot numbers as they appear in the identification chart presented in Figure 1. Columns 2 and 3 give the approximate offset positions of the observed spots measured in seconds of arc from the central "star" of the nebula. Positive numbers are used for north and west offsets. Because of large entrance apertures used (65" ≈ 4mm at the 36-inch telescope) it was necessary to determine if the photocathode was being uniformly illuminated from all positions in the apertures. The response of the photocathode, as a function of position in the aperture, was mapped by drifting a bright star across the diaphragm in the EW direction at several NS positions along the diaphragm. It was found that only the 65" fields at H_α were severely vignetted; the light loss for the other aperture-grating angle combinations was found to be less than 4 percent for a uniformly illuminating light source. Since it was not possible to correct the 65" H_α observations without a

detailed knowledge of the brightness distribution of the observed areas, the results are presented in Table 1 for comparison but will not be used in the discussion and interpretation of the observations. In what follows, $F(\lambda)$ will be used to denote the observed fluxes and $I(\lambda)$ the emitted ones. Column 6 of Table 1 presents the logarithmic extinction correction at H_β, $C(H_\beta)$ defined as $C(H_\beta) = \log I(H_\beta) - \log F(H_\beta)$ and calculated from the expression

$$\log F(\lambda)/F(H_\beta) = \log I(\lambda)/I(H_\beta)+C(H_\beta)f(\lambda) \quad (1)$$

where the observed $F(H_\gamma)/F(H_\beta)$ line ratios have been used together with the theoretical ratio $\log I(H_\gamma)/I(H_\beta) = 0.329$ calculated by Blocklehurst (1971) for a case B nebula at $10^{4\circ}$ K. It is important to remark that $C(H_\beta)$ represents the extinction only if the dust is in front of the nebula and unmixed with the gas (see discussion in Paper II). The Whitford reddening function $f(\lambda)$ has been used in equation 1 to derive the values of $C_{\beta\gamma}(H_\beta)$. The values of $C(H_\beta)$ determined from the $F(H_\alpha)/F(H_\beta)$ and the $F(H_\beta)/F(H_\gamma)$ line ratios are presented in Table 2 for the 32".5 observations. The last column in each table presents the corresponding absolute H_β fluxes uncorrected for reddening.

The observational errors associated with the logarithmic line ratios and $\log I(H_\beta)$ have been estimated from repeated observations of 10 spots on different nights,

to be 0.02 and 0.05 respectively.

Both the 65" and the 32".5 observations of H_α are contaminated by the [NII] lines at 6583Å and 6548Å. Peimbert and Torres-Peimbert (1974) find that in the brightest parts of the nebula, the stronger of these lines, at 6583Å, is about ten times weaker than H_α. Monochromatic images of the nebula in the light of H_α and [NII] presented in Figures 2 and 4 show that the ratio $F(H_\alpha)/F([NII])$ is very low throughout the nebula. The plates were obtained with the 40-inch Yale telescope at CTIO using an electrostatically focussed image tube and the Tololo H_α LMC and [NII] LMC interference filters. Both filters have peak transmissions of 55 percent and their FWHM (full width at half maximum) are very similar (15Å and 14Å respectively). Both plates were exposed for 60 minutes on N_2-baked IIIa-J emulsion and developed together. The [NII] plate is also reproduced in Figure 4 together with a 15 minute H_α photograph of the nebula obtained using the equipment described above. From the monochromatic imagery and the photoelectric observations of Peimbert and Torres-Peimbert, it is concluded that a correction of 10 percent should be applied to the observed H_α fluxes in order to determine the correct Balmer decrements.

b) Fabry-Perot Observations

Smith and Weedman (1972) have carried out an extensive

mapping of the velocity structure of 30 Doradus, using a pressure scanned Fabry-Perot interferometer to determine [OIII] λ5007-line profiles at numerous positions in the nebula. These authors also obtained a number of H_α line profiles through a 30" field stop, which are mostly unpublished. For the purpose of establishing to what an extent the kinematical properties of the nebula are interrelated with its surface brightness distribution, as determined above, the unpublished H_α line profiles were obtained from Dr. Smith. The raw data were reduced by fitting the profiles with Gaussian functions in the same way as discussed in Paper I. Nearly one-fourth of the profiles were non-Gaussian and could not be used. The results for the remaining 26 locations in the nebula are presented in Table 3 as follows: column 1 presents the spot designation as given by Smith and Weedman (1972); columns 2 and 3 show the peak count above the continuum level I_o, and the e-folding widths of the profiles β_o determined from the least squares fits. The turbulent component of the profile widths V_{turb} defined in Paper I as

$$V^2_{turb} = \beta_o^2 - \beta_i^2 - \beta_{th}^2$$

where β_i is the width of the instrumental profile, measured by Smith and Weedman to be $\beta_i = 6.3$ km sec^{-1} and β_{th} is the component of the observed width due to thermal motions of the gas. The last column of Table 3 presents the H_α

magnitude of the observed area calculated as:

$$m_{H\alpha} = -2.5 \log(\int F_{\alpha}^{*}(\lambda)d\lambda) + 20 - \eta\chi - A(H_{\alpha}) + \text{const}$$

where $F_{\alpha}^{*}(\lambda)$ is the H_{α} line profile deconvolved from instrumental broadening, η is the atmospheric extinction coefficient or about 0.08 mag/airmass and χ is the airmass. The interstellar reddening correction $A(H_{\alpha})$ was derived assuming that all the extinction comes from dust in front of the nebula. For Whitford's extinction law $A(H\alpha) = 1.67C(H_{\beta})$. The normalization constant was determined by reducing all magnitudes to the night of December 17, 1970, using the photometric observations presented above.

c) Comparison with Radio Continuum Observations

It was found in Paper II, that dust and gas coexist within giant extragalactic HII regions. This implies that, in general, the use of Eq. (1) to determine the extinction "corrections" will lead to a gross underestimation of the true emitted fluxes $I(H_{\beta})$. Since the radio continuum fluxes are not affected by dust extinction, a comparison between radio and H_{β} observations provides the means to determine the physical parameters of the HII region and the extent to which dust and gas within the nebula may be intermixed. In the case of 30 Doradus this comparison is complicated by the possible presence of a non-thermal component in the observed centimeter radiation, as suggested by Mathewson and Healey (1964) and Le Marne (1968). In addition, the

H_β photometry reported above covers only part of the nebula and thus an extrapolation is necessary to derive the integrated fluxes. For these reasons, the comparison between radio and H_β fluxes, presented in Table 4, leads to uncertain results and the parameters derived for the halo must be considered upper limits. As in Paper II, the comparison has been done separately for the core and for the halo to stress their differences. The first column of the table containing the linear diameters of the core and of the outermost parts of the nebula determined from the photograph reproduced in Figure 1, and adopting a distance of 52.2 kpc to the LMC (Gascoigne 1969). Notice that the linear diameters are significantly smaller than those given by Sandage and Tammann (1974a) for the entire 30 Doradus complex. Column 2 of Table 4 is the 21cm continuum flux as measured by Mathewson and Healey (1964), in the core and halo, and have dimensions almost identical to those determined optically. Column 3 gives the H_β fluxes of each component extrapolated from the observations presented in Table 1. The radio and optically derived absorption corrections at H_β, $A(H_\beta) = 2.5C(H_\beta)$ are presented in columns 4 and 5. The radio derived extinctions have been determined in the same way as described in Paper II. Notice that $A(H_\beta)$ for the halo is very large, possibly due to the presence of the non-thermal component. The physical

parameters of the core and the halo that can be directly derived from the observations are presented in the remaining columns. The ionizing flux of the exciting stars is $S_u(0)$; the number of 05 stars as defined by Searle's (1971) model required to produce $S_u(0)$ is N_s. The derived electron densities, n_e, of the core and the halo, assuming that both components are uniformly filled with gas, are given in the last two columns of Table 4. It is clear from Figure 1 that only a small fraction of the volume occupied by the nebular halo is filled with gas, and that in consequence the actual electron densities must be significantly higher.

III. DISCUSSION

a) Core-Halo-Structure

The core-halo model generally used to describe the radio continuum observations of giant extragalactic HII regions (Israel 1975) was originally proposed by Mathewson and Healey (1964) to represent the radio structure of 30 Doradus. The core and the envelope of the nebula can be clearly distinguished on the photographs reproduced in Figures 1 and 2. The dimensions of the two optical components (§IIc) very closely correspond to those of their radio counterparts.

Because of the proximity of 30 Doradus, it is possible to establish the relation between the optical appearance of the nebula and the distribution of stars that may produce its ionization. In this section the interrelation between ionized gas and the stars will be established on the basis of photographic plates of the nebula taken with the 40-inch telescope of the Carnegie Southern Observatory at Las Campanas.

The photograph reproduced in Figure 1 is a 120 minute exposure taken on 098-04 emulsion behind a Schott RG1 filter. The core, which appears completely burned out in the center of the nebula, can be clearly distinguished from the halo which presents an intricate structure composed of giant loops and filaments. The core-envelope structure is also very clearly exposed on the H_α photograph presented in Figure 2.

Figure 3 presents reproductions of two plates of the nebula exposed for 5 and 30 minutes on 103a-D emulsion through a Schott GG485 filter. It is possible to see the individual stars on the plates that are exciting the gas in both the core and the envelope. The stars in the halo will be considered first. Upon close examination of the 30 minute plate reproduced in Figure 3, it is possible to see that the gas in the envelope very closely delineates the distribution of stars imbedded therein. The presence of fine filamentary structure and dense nebulosity around many of the

stars indicate that they must be physically connected with the nebula rather than superimposed on the line of sight. A particularly noteworthy example of the association between gas and stars has been marked L on Figure 3. The stars, apparently associated with the gas in this gigantic loop in the southern end of the nebula, form an "M" shaped pattern which is very closely followed by the distribution of ionized gas. In fact, it can be seen that the whole loop is delineated by stars. It may be concluded, therefore, that this loop as well as some of the others that present the same characteristics are superpositions of Strömgren "spheres" around individual stars. An example of one such Strömgren sphere, which is not associated with the large-scale structure of the nebula, has been illustrated in Figure 3. The exciting star, marked "S" on the short-exposure photograph, appears surrounded by a compact HII region on the 30 minute plate. The HII region can be seen on the H_α photograph presented in Figure 2, to have a diameter of nearly 20 seconds of arc or about 5 parsecs, the size of the Orion Nebula! Many other similar examples can be found by comparing the two photographs of Figure 3, a few of which have been pointed out by Feast (1961).

To demonstrate quantitatively the degree to which individual stars in the halo are responsible for its ionization, the catalogues of bright stars in the LMC by Feast et al. (1960), Sanduleak (1968), and Fehrenbach and Duflot

(1970) were searched for O, B, and Wolf-Rayet stars within 15' of the nebular center. Eight stars were found in the core and another eight were located in the halo. The parameters for the eight halo stars are summarized in Table 5. The first column of the table gives the Sanduleak (1968) number of the star which has been used for identification in Figure 3. The spectral types of the stars as determined by Feast et al. (1960), Ardeberg et al. (1972), and Westerlund and Smith (1964) is given in column 2. The absolute magnitudes of the stars determined from the photoelectric photometry of Ardeberg et al. (1972) and Isserstadt (1975), and using a distance modulus of 18.59 to the LMC is listed in column 3. A uniform reddening correction $A_V = 0^m.5$ was used for the eight halo stars (cf §IIIb). The ratio $S_u(0)/\pi F_V$ between the Lyman continuum photon fluxes and the visual luminosity of the star as determined by Morton (1970) for galactic WR stars is given in column 4. The $S_u(0)/\pi F_V$ ratio for WN+O stars was determined averaging the values for WN stars given by Morton (1970) and for O stars given by Thuan (1975).

The photon fluxes emitted by the stars shortward of the Lyman limit, $S_u(0)$, is given in column 5. The fluxes for the O and B stars have been taken from Thuan's (1975) compilation of model atmospheres calculations. The ionizing fluxes for the WN and WN+O stars were calculated from the

$S_u(0)/\pi F_V$ ratios and the absolute visual magnitudes. The ionization parameter $Rn_e^{2/3}$ of a dust-free HII region of Strömgren radius R and uniform electron density n_e around each star is shown in column 6.

Finally, the corresponding Strömgren radius if $n_e = 20\ cm^{-3}$ (cf Table 4) is given in the last column. These radii have been drawn around each individual star in Figure 3. Most of these stars appear to be surrounded by nebulosity (cf Figures 2 and 3) and therefore are likely to be associated with the gas. This is not the case, however, for stars S138 and S140 in the northern part of the nebula. On the other hand, it can be seen in Figures 1 and 3 that these stars delineate very closely the long, thin filament stretching in the northernmost parts of the nebula. It is therefore very difficult to believe that they are only superimposed on the filament and not physically connected with it. It is of interest to remark that the strong magnetic field apparently associated with the nebula, according to Mathewson and Ford (1970) and Isserstadt and Reinhardt (1976) seems to stretch along the filament. If the measurements are correct, there is a basis to conjecture that the ionized gas is streaming along the filament. The long filament which characterizes the westernmost part of the nebula (Figure 1) also appears to stretch along the magnetic field lines in that region. It seems appropriate

therefore, to assume that the large-scale filamentary structure of the nebula is defined by the strong radial magnetic field associated with the nebula as a whole. The roles played by the magnetic field and by the stellar distribution in defining the spatial structure of the nebular halo appears thus clearly delineated.

There is yet a third important effect that must be considered: stellar winds. It has been established observationally (Morton 1967; Smith 1970; Conti and Leep 1974; Snow and Morton 1976) that stars of spectral types earlier than B2 and brighter than $M_V \simeq -6.0$ may have strong stellar winds characterized by velocities of the order of 2500 km sec^{-1} and mass loss rates up to 10^{-6} $M_\odot$/yr. In particular, Wolf-Rayet stars are known to have massive winds (Underhill 1968). It is relevant thus to notice that 30 Doradus shows several sharp loops that may in fact be "bubbles", similar to those that have been discussed by several authors in connection with the interstellar medium (see Castor et al. 1975 and references therein). In particular, the gigantic loop characterizing the eastern part of the nebula presents an extremely sharp inner edge and appears to be centered on the WR star S248. It has been shown by Castor et al. (1975) that as the wind "plows" through the nebular gas, a shock front will develop which will expand outwards from the star. At any given time the distance from the shock

front to the driving star will be given by

$$r(t) = a\left(\frac{\varepsilon L_*}{\rho}\right)^{1/5} t^{3/5} \qquad (2)$$

where L_* is the luminosity of the star, ρ is the mass density of the surrounding gas, the parameter ε represents the fraction of the stellar energy flux being deposited on the wind, and a is a numerical constant of order unity. Typical values for WR stars are $\varepsilon \simeq 0.01$ (Underhill 1968). The radius of the eastern loop determined from Figure 1 is $r(t_o) \sim 40$ pc. Assuming a pure hydrogen nebula and a particle density of 20 cm^{-3} (Table 4), the age of the loop t_o is found from equation (2) to be about 10^6 years, if the luminosity of S248 is determined using the results of Table 5, and assuming a blackbody bolometric correction with $T_* = 30000°$ K (Morton 1970). The age thus calculated is less than the main-sequence lifetime of the exciting stars and does not seem to contradict any observational evidence. The velocity of expansion of the "bubble" is given by

$$v(t) = 3/5\ a\left(\frac{\varepsilon L_*}{\rho t^2}\right)^{1/5} \qquad (3)$$

which, for the parameters assumed before and $t = 10^6$ years, gives $v(t_o) = 20$ km sec^{-1}.

At four positions within the loop, profiles of [OIII] λ5007 obtained by Smith and Weedman (1972) are double-peaked, indicating an expansion velocity on the average of 30 km sec^{-1}, in reasonably good agreement with the

calculated value.

If all the dust and gas that were originally within the Strömgren sphere around the star are assumed to be at present within the HII circumstellar shell, an expression for the thickness ℓ of the shell can be determined equating the ram pressure on the expanding "bubble" to the internal kinetic pressure of the gas within the shell. The result is

$$\ell = \frac{(Rn_e^{2/3})^3 \, kT_e}{n_e^2 V^2 \, \mu r^2}$$

where n_e is the electron density of the gas outside the "bubble" and μ is the mean atomic weight of the gas. Using the observed radius of the shell r, the observed expansion velocity v, $Rn_e^{2/3}$ for S248 as given in Table 5, and an electron temperature $T_e = 10^{4\circ}$ K, a thickness of 0.2 pc is derived. This is in reasonable agreement with the measured value of about 0.6 pc (cf Figures 1 and 2). Figure 6 shows that the dust is also denser within the boundaries of the "bubble".

There is another remarkably thin loop in the north-eastern part of the nebula, which appears to be centered on a star located southwest of S246 (cf Figure 3). Its radius is comparable to that of the S248 loop. The [OIII] profiles obtained by Smith and Weedman within this loop are also double indicating expansion velocities of the order of

20 km sec^{-1}.

There appears to be, thus, observational evidence for the role that stellar winds may play in determining the spatial structure of the envelope of 30 Doradus. It may therefore be concluded that the structure of the halo of 30 Doradus is determined primarily by the distribution of exciting stars imbedded therein and is modeled both by the magnetic fields associated with the nebula and by strong stellar winds. In a general way, the loops seem to be formed by stellar winds and the filaments by the magnetic fields.

The complicated structure of the nebular core can be fully appreciated on short exposure photographs such as the ones reproduced in Figures 3 and 4. The short exposure plate of Figure 3 shows tens of stars imbedded in the core of 30 Doradus. At least fifty stars are easily seen in the central cluster, and, on the original many more appear, almost completely obscured by dust. The ionizing fluxes of the eight stars in the core observed by Feast et al. (1960) have been determined using the procedure described above. For four of the stars the absolute magnitudes were estimated using the photometry by Feast et al. (1960) and Westerlund and Smith (1964), including the central "star" of the nebula R136. The magnitudes for the remaining four have been estimated by eye on short exposure plates. It is practically

impossible to accurately measure the magnitudes of the stars in the core due to the severe crowding and to contamination by emission lines from the nebula. Consequently, the average magnitudes for WR stars in the LMC determined by Smith (1968) were used to compute the ionization fluxes of the core stars. These "adopted" magnitudes are listed in column 5 of Table 6. The ionizing flux of the central object R136 is seen to be nearly one hundred times larger than that of O5 stars (Searle 1971; Thuan 1975). Since the spectral classification of this star is known only approximately, and since the ionization fluxes may vary by factors of as much as 100 from WN5 to WN8 stars (Morton 1970), the large ionizing fluxes derived for R136 cannot be unequivocally interpreted. Even if the luminosity of R136 has been overestimated by a factor of 50 in Table 6, a mass larger than 100 $M_{\odot}$ would be required to balance the radiation pressure. Moreover, Feast (1961) and Westerlund and Smith (1964) have suggested that R136 may be a composite object. Were that the case, since the various stars forming R136 are likely to have different temperatures, the use of the integrated absolute magnitude would lead in general to an overestimate of the ionizing flux. No evidence of a composite nature for R136 is contained in the plates reproduced in Figures 3 and 4.

It is of interest to notice that the UV observations

of the nebula by the ANS satellite (Israel 1976) seem to indicate the presence of a hot, superluminous object in the nebular core. The Fabry-Perot observations of Smith and Weedman (1972) show that all of their [OIII] line profiles within 8 pc of R136 are double-peaked, with an average separation between the two components of 45 ± 2 km sec^{-1}. The mean radial velocity of the profiles in the central regions is 270 km sec^{-1}, very close to the mean velocity of 269 km sec^{-1} they derive for the nebula as a whole. Following the arguments presented above, the double nature of the profiles is taken as an indication of a strong wind, driven by R136 with the gas expanding in the central regions at a velocity of 23 km sec^{-1}. A similar conclusion was reached by Smith and Weedman. From the observed velocities and equation (3) with $t = 10^6$ years, one gets $L = 10^{37}\ n_e$ ergs. With $n_e = 100$ derived in Table 4 for the nebular core, $L = 10^{40}$ ergs sec^{-1}. This result is consistent with the luminosity of 9×10^{39} ergs sec^{-1} derived for R136, assuming a bolometric correction of -2.5 appropriate to a blackbody of 35000° K. It should be noticed, however, that the implied luminosity corresponds to the Eddington limit for a star of 1000 solar masses.

Clearly, further observations of this "star" should be pursued. They may lead to a better understanding of the nature of supermassive Wolf-Rayet stars and of the inter-

action between strong stellar winds and a surrounding medium.

Assuming that the Lyman continuum fluxes of Table 6 for WN+O stars are not greatly overestimated, the total ionization fluxes from the eight core stars considered, is only three times less than the total UV flux required to explain the observed radio fluxes (cf Table 4). Since there are at least fifty to a hundred stars visible in the central cluster of 30 Doradus, there is no reason to believe that the ionization of the core is due to any source other than the large number of stars therein imbedded.

The intricate filamentary structure of the brightest parts of the core can be fully appreciated on the monochromatic images of the nebula presented in Figure 4. In addition to the [NII] and H_α photographs already discussed in §IIa, images in the light of OI λ8446-47 and [OI] λ6300 have been reproduced in that figure. The original intention for obtaining these images was to trace high density HII-HI transition zones in the nebula. In these dense boundaries, the intensity of the OI λ8446 (3^3P-2^2S) multiplet will be greatly enhanced over the [OI] λ6300 emission by fluorescent absorption of hydrogen L_β photons to the 3^3D level, followed by radiative decay to the 3^3P level (Münch and Taylor 1974). The efficiency of the narrow-band interference filters used (20Å and 12 Å FWHM respectively) was, however, greatly

reduced due to the redshift of the lines. This effect, combined with the fact that the neutral oxygen lines are among the weakest nebular lines observed (Peimbert and Torres-Peimbert 1974) make it very difficult to detect the high density boundaries on the available photographs. Comparison between the OI and [OI] photographs presented in Figure 4, however, shows the presence of a weak filamentary structure on the λ8446 image not present on the λ6300 plate. In particular, the long filament on the eastern part of the core, prominent on the H_α plate, can be clearly distinguished on the λ8446 photograph. The filamentary structure, however, has completely disappeared on the λ6300 plate. This suggests that the filaments may be dense interfaces between neutral and ionized hydrogen. Clearly, however, the quality of the monochromatic OI and [OI] imagery available precludes any further conclusions.

Partly due to the fact that the emission lines have been redshifted out of the bandpasses, and partly due to the absence of strong emission lines near λ6300 and λ8446, the stars of the central cluster are very clearly visible on these plates. By comparing these images with the H_α photograph reproduced in the figure, it is seen that the gas and the stars are very closely related.

To summarize, the photographic evidence presented above supports the conclusion that both the core and the halo are

being ionized by stars. The stars responsible for the ionization of the halo do not appear to be directly related to the central cluster, the source of ionization for the dense core. Both the core and the halo can be regarded as superpositions of "Strömgren spheres". The dynamical properties of these "clusters" of HII regions will be discussed in §IV.

b) The Reddening Law of Nebular Light

The observations presented in Paper II showed that there are significant amounts of dust imbedded within giant HII regions. This conclusion was prompted by the large extinctions required to explain the 21 cm radio continuum observations as compared with the systematically lower values determined from the Balmer decrements. On the basis of the correlation found between reddening and surface brightness within the HII regions, it was possible to interpret the discrepancy in terms of large amounts of dust within the nebulae.

It can be seen from the results presented in Tables 1, 2 and 4 that the same situation is found from the observations of 30 Doradus. Figure 5 shows a schematic representation of the reddening distribution over the nebula. A comparison between Figures 1 and 5 shows immediately that the brightest parts of the nebula are also the most reddened. A similar result was found by Faulkner (1967) who showed

that the brighter isophotes of the nebula, determined photographically, correspond to the isophotes of higher reddening. No interpretation was given by Faulkner, however, to the correlation.

The correlation between brightness and reddening in the Orion nebula have been analyzed by Münch and Persson (1971) through means of the function

$$\phi = \Delta\log\,[F(H_\beta)]\;\Delta\log\,[F(H_\beta)/F(H_\gamma)]$$

where $\Delta\log\,[F(H_\beta)]$ is the difference in surface brightness and $\Delta\log\,[I(H_\beta)/I(H_\gamma)]$ the difference in reddening between two locations in the nebula. Clearly, if $I(H_\beta)$ and reddening are uncorrelated and fluctuate randomly, the distribution of values of ϕ over the entire nebula will be symmetrical about zero. On the other hand, if $\Delta\log\,[F(H_\beta)]$ and $\Delta\log\,[F(H_\beta)/F(H_\gamma)]$ are well correlated, there should be an excess of positive values of ϕ. The observations of 30 Doradus presented in Table 1 have been used to construct the histogram presented in Figure 6. It can be seen that the distribution is very strongly peaked at zero and is clearly skewed towards positive values of ϕ. The large number of zero values arises from the fact that most of the observed places in the nebula are in the halo, where the correlation is expected to be weaker.

In view of these results and the results of Faulkner (1967), the large extinction required to explain the radio

observations of 30 Doradus presented in Table 4 is interpreted as due to the presence of dust within the nebula.

It is now possible to apply the results obtained in Paper II for a mixed distribution of dust and gas, to establish the reddening function of the dust grains.

For a mixed configuration of dust and gas in which the dust-to-gas ratio tends to a constant value, the ratio between the observed intensities of the Balmer lines will tend to a limiting value as the dust optical depth tends to infinity. This value was found in Paper II to be

$$\frac{F(H_\alpha)}{F(H_\beta)} = 2.85 \frac{f(\beta)}{f(\alpha)} e^{-(\tau_\alpha^{ext} - \tau_\beta^{ext})}$$

where $f(\lambda)$ represents the reddening function of the dust grains. Similarly it is easy to verify that

$$\frac{F(H_\beta)}{F(H_\gamma)} = 2.13 \frac{f(\gamma)}{f(\beta)} e^{-(\tau_\beta^{ext} - \tau_\gamma^{ext})} \quad . \qquad (4)$$

Here τ^{ext} represents the optical depth of the dust located in front of the nebula. For 30 Doradus, τ^{ext} can be determined in several ways. The lowest observed Balmer decrements of Table 1 and 2 indicate that $E(B-V)_{ext} \lesssim 0^m.1$. The same result is obtained from Faulkner's (1967) isophotes of the outer parts of the nebula. A similar reddening was found by Feast et al. (1960) from photometry of bright stars in the vicinity of 30 Doradus. Finally, Gascoigne (1969)

finds a color excess $E(B-V) = 0^m.08$ in the direction of the LMC. Assuming $E(B-V) = 0^m.1$ in front of the nebula, then $C(H_\beta)_{ext} = 1.21\ E(B-V)$ gives 0.12 and $e^{-(\tau_\alpha^{ext} - \tau_\beta^{ext})} \equiv 10^{C(H_\beta)_{ext} f(\alpha)}$ gives 1.10. Similarly, $e^{-(\tau_\beta^{ext} - \tau_\gamma^{ext})}$ gives 1.04.

The maximum values of $\log[F(H_\alpha)/F(H_\beta)]$ and $\log[F(H_\beta)/F(H_\gamma)]$ found for 30 Doradus in Tables 1 and 2 excluding spots 11 and 12* are

$$\log [F(H_\alpha)/F(H_\beta)]_{max} = 0.66 \text{ and } \log [F(H_\beta)/F(H_\gamma)]_{max} = 0.34.$$

---

*These positions have been excluded because the stars R134 and R136 were included with #11, and S246 was included by #12. Since these are Wolf-Rayet stars, the broad He II lines near H_α and H_β will alter significantly the Balmer decrements at these positions.

From these values, the ratios of $f(\beta)/f(\alpha)$ and $f(\gamma)/f(\beta)$ can be calculated using equation (4) after correcting the H_α fluxes for contamination by the [NII] lines as described in §IIa. The results are compared in Table 7 with the predicted values calculated by Münch and Persson (1971) for Whitford's and for Whiteoak's (1966) reddening laws for the Orion Nebula.

Further information about the reddening properties and the spatial distribution of the dust grains in the nebula

can be obtained by means of a two-color plot. In a plot of log $[F(H_\alpha)/F(H_\beta)]$ against log $[F(H_\beta)/F(H_\gamma)]$ a particular configuration of dust and gas will be represented by a point. If the dust is in front of the nebula and unmixed with the gas, the various points in the two-color plane representing the various positions observed in the nebula will follow along a straight line or "reddening track" of slope (cf eq. [1]).

$$\Delta_u = \frac{f(\gamma)-f(\beta)}{f(\beta)-f(\alpha)}$$

On the other hand, in a well mixed gas-dust configuration with infinite optical depth, the slope of the reddening tracks can be seen from equations (3) and (4) to be

$$\Delta_m(\infty) = \frac{\log f(\gamma)-\log f(\beta)}{\log f(\beta)-\log f(\alpha)} \quad .$$

An arbitrary dust-gas distribution will define a region in the two-color plane bounded by two straight lines of slopes Δ_u and $\Delta_m(\infty)$ passing through the recombination points (Münch and Persson 1971). The two-color plot for 30 Doradus determined from the observations presented in Table 2 is shown in Figure 7, which contains the recombination points of Burgess (1958) and Blocklehurst (1971). The least squares line of slope of 0.23 ± 0.06 (rms), shown in that figure, is seen to pass within one percent of the Blocklehurst point and slightly farther away from the Burgess point.

The values of Δ_u and $\Delta_m(\infty)$ calculated by Münch and Persson for the different extinction laws is given in Table 7. It can be seen that, as was expected, the observed slope is significantly lower than the slopes predicted by any of the reddening laws for an unmixed dust-gas configuration. It follows that the observed distribution of reddening along the various lines of sight in the nebula must be bounded by two straight lines of slopes Δ_u and $\Delta_m(\infty)$. A straight-line least squares fit through the data would then yield a slope Δ such that

$$\Delta_m(\infty) < \Delta < \Delta_u \qquad (5)$$

provided that the different configurations cover a significant range in the two-color plot variables (Münch and Persson 1971). The results of Table 2 show that this is clearly so for 30 Doradus. Thus, it can be seen in Table 7 that Whitford's extinction law cannot satisfy the above inequality. Moreover, the observed ratios between the values of the reddening function at the wavelengths of the Balmer lines are significantly lower than those predicted by the normal extinction law as presented in Table 7. That table shows that the observed slope and reddening function ratios are best fit by an extinction law similar to that found in the Orion Nebula with $R = A_V/E(B-V)$, the ratio of total to selective absorption equal to 5. The observational errors do not exclude the values $R \gtrsim 7$. These values of R,

however, are unlikely since the region allowed by the inequality (5) would become quite narrow and many of the observed points would fall outside the limits of this region. On the basis of the observed slope and reddening function ratios presented in Table 7, it is therefore concluded that the reddening law followed by the dust grains in 30 Doradus, and in other extragalactic HII regions, is similar to that found for the stars imbedded in the Orion Nebula by Whiteoak (1966), and for the Orion nebular light by Münch and Persson (1971), with R = 5.

IV. DYNAMICS

The heuristic dynamical model for giant HII regions outlined in Paper I and mentioned in §III of this Paper will be further developed here and compared with the observations of 30 Doradus. In this model, giant HII regions are assumed to be clusters of HII regions around the hundreds of ionizing stars imbedded in the nebulae. Many such "Strömgren spheres" can be seen directly on the photographs of 30 Doradus presented in the previous section.

Each member of the "cluster" will be assumed to have properties similar to the Orion Nebula. The kinematical data relevant for Orion and for 30 Doradus and NGC 604 will be presented here. Throughout the discussion the word "turbulence" will be used to describe the state of

motion of the gas in the nebulae. On the other hand, a hierarchy of eddies at various scales and high Reynolds numbers will be referred to as "fluid dynamical turbulence".

a) Observations

The comparison of the available kinematical data for 30 Doradus, NGC 604 and the Orion Nebula, given in Table 8, shows that there are clear similarities among the three nebulae, i.e., 1) All three (and in fact most galactic and extragalactic HII regions) are associated with large HI clouds, presumably out of which they were originally formed. 2) The radial velocities determined from the optical emission lines are systematically larger than those determined from the 21 cm line from the surrounding cloud. This feature is most readily interpreted as an expansion of the HII region against the neutral surrounding material. 3) The observed widths of the H109α lines are significantly larger than the widths of the optical recombination lines. This is almost certainly not due to Stark broadening of the high n line. For electron densities of less than 10^4 cm^{-3}, the Stark profile is about one order of magnitude narrower than the turbulent broadening at 20-30 km sec^{-1} (Terzian 1974). 4) The width of the 21 cm line indicates turbulent motions in the neutral gas comparable to those derived for the HII regions from the H109α observations. The consequen-

ces and possible interpretation of these results will be discussed below.

There are two major differences between 30 Doradus and the Orion Nebula: the dimensions, Orion being more than 50 times smaller than 30 Doradus, and the magnitude of the observed motions. All single peaked profiles of the Orion Nebula determined by Wilson et al. (1959) and Smith and Weedman (1970) correspond to subsonic motions. The profiles of 30 Doradus, on the other hand, indicate highly supersonic turbulent velocities. In addition, there are other differences of a more involved nature. To describe them, the 13" and 30" observations by Smith and Weedman (1972) of 30 Doradus will be used unless otherwise stated. The differences are:

1) Fluctuations in the profile widths. Excluding double peaked profiles, fluctuations as large as 15 to 20 km sec^{-1} are seen in 30 Doradus at different positions (cf Table 3). By contrast, in the Orion Nebula the fluctuations are at most 3-4 km sec^{-1} (Wilson et al. 1959; Smith and Weedman 1970).

2) Correlation between V_{turb} and surface brightness. A plot of H_α surface brightness against turbulent velocity at the various positions of the 30 Doradus Nebula, as given in Table 3, is shown in Figure 8. It is seen that the brightest parts of the nebula also appear to be the most turbulent. The uncertainties involved in the H_α magnitudes, however, pre-

clude the determination of a quantitative relation between surface brightness and turbulent velocity. A similar correlation for the Orion Nebula has never been published.

3) The spatial distribution of radial velociries. The differences in radial velocity between two points on the 30 Doradus Nebula $(\Delta V)^2=(V_A-V_B)^2$, averaged over all pairs of points separated by a projected distance λ, have been plotted in Figure 9 against λ. Typically, each plotted point represents an average of 100 pairs for values of λ less than 160" and of 50-80 pairs for larger separations. The rms deviations from the mean values are also shown in Figure 9. Since the double peaked profiles indicate strong expansion velocities which dominate over the turbulent motions (cf §IIIa) they have not been included in the computation of the average $(\Delta V)^2$, which will be denoted $<(\Delta V)^2>$.

The observed correlation of Figure 9 is well represented by the functional relations

$$<(\Delta V)^2> = C^2\lambda \quad \text{for } \lambda < 30 \text{ pc},$$

with $C^2 = 20 \text{ km}^2\text{sec}^{-2}\text{pc}^{-1}$, and, (6)

$$<(\Delta V)^2> = \text{Const. for } \lambda > 30 \text{ pc}.$$

In the case of the Orion Nebula, the empirical correlation of velocities has been shown by Von Hörner (1951) and Münch (1958) to be

$$<(\Delta V)^2> = C^2\lambda^{2/3} \quad \text{for } 0.003 < \lambda < 0.3 \text{ pc},$$

with $C = 10 \text{ km sec}^{-1}\text{pc}^{-1/3}$, and has been interpreted as the

consequence of compressible turbulence. It will be shown below that this interpretation cannot be used in the case of 30 Doradus.

The limit of 30 parsecs beyond which $<(\Delta V)^2>$ = Const. in the 30 Doradus Nebula will be called the physical core size of the nebula and denoted by Λ. It corresponds to the distance that a gas element moving at 30 km sec^{-1} will travel in 10^6 years.

b) Discussion

Because the observed motions in 30 Doradus are highly supersonic, fluid dynamical turbulence involving a superposition of whirls of different sizes, will decay very rapidly. The stars, which are the only obvious source of energy available to restore the motions can only do it in time scales comparable to their main-sequence life (Paper II). Consequently, no supersonic motions could be expected on these HII regions on this account, contrary to what is observed.

One must conclude therefore, that either another mechanism must be operating to maintain the observed supersonic motions, or that the observed turbulence reflects large scale motions in the HII regions with very low collision rates. This possibility is also suggested by the observed fluctuations in the line profile widths.

In this section the observed motions will be analyzed

in terms of the cluster model in which giant HII regions are aggregates or "clusters" of hundreds of Orion-like HII regions. Each component-nebula will be assumed to be moving together with its ionizing star, and the observed net turbulence will ultimately reflect the motions of the exciting stars. Each component will be considered to be optically thick by dust to the optical radiation from the other components and it will be assumed that there is very little dust and gas outside the members of the "cluster"

Let us consider the properties of the HII region cluster in a quantitative way. The intensity distribution in velocity of any component will be assumed to have the form

$$I(v) = I_o e^{-v^2/\beta^2}$$

where I_o and β are the same for all components. The intensity distribution along the line of sight at position A in the nebula will be given by

$$I_A(v) = \sum_{i=1}^{N_A} I_o e^{-(v_i - v)^2/\beta^2} e^{-\tau_i} \qquad (7)$$

where the extinction optical depth τ_i of the i-th component will be assumed to be proportional to the linear dimension s_i: $\tau_i = \kappa(\lambda) s_i$. All velocities will be considered with respect to the rest frame of the "cluster" nebula. For 30 Doradus, this velocity will be assumed to be the mean velocity of all profiles or 269 km sec^{-1}.

The mean radial velocity integrated along the line of sight at A is given by

$$V_A = \frac{1}{Q}\int_{-\infty}^{+\infty} I_A(v)\,v\,dv = \sum_{i=1}^{N_A} v_i e^{-\kappa(\lambda)s_i} \Big/ \sum_{i=1}^{N_A} e^{-\kappa(\lambda)s_i} \quad ,$$

where $Q = \int I_A(v)\,dv$. The rms spread in velocities around the mean will similarily be

$$\sigma_A^2 = \left\{ \sum_{i=1}^{N_A} (v_i - V_A)^2 e^{-\kappa(\lambda)s_i} \Big/ \sum_{i=1}^{N_A} e^{-\kappa(\lambda)s_i} \right\} + \beta^2/2 \ .$$

The observations show that at any given position in the nebula, the widths of the profiles obtained through a 13" aperture are the same as the widths of the profiles taken on a 30" field. This means that a large number of elements must be encompassed along any given line of sight. For simplicity therefore, the summations in eq. (8) will be replaced by integrations. Since the optical depth becomes very large as $\tau \to \Lambda$, the integrations will be continued to infinite s. Now the formulation becomes identical to that given by Münch (1958) in his study of the Orion Nebula. The average profile width over all positions in the HII region is given by (Münch 1968)

$$\langle \sigma_A^2 \rangle - \frac{\beta^2}{2} = \int_0^\infty\int_0^\infty e^{-\kappa(s_1+s_2)} B(s_1,s_2)\,ds_1 ds_2 . \qquad (9)$$

Here $B(s_1,s_2)$ is the "structural function" of the fluid defined as

$$B(s_1,s_2) = \langle (V_A(s_1) - V_A(s_2))^2 \rangle_{av} \quad ,$$

where now the averaging is carried out over all lines of sight. The structural function is related to the projected

velocity correlation $<(\Delta V)^2>$ by the equation (Kaplan 1966)

$$<(\Delta V)^2>=\kappa^2 \iint e^{-\kappa(s_1+s_2)}\{B[\lambda^2+(s_1+s_2)^2]^{1/2}-B(|s_1-s_2|)\}ds_1 ds_2 \tag{10}$$

where λ is the projected separation between the gas elements. Assuming that $B(s_1,s_2)$ has the form $C^2(|s_1-s_2|)^\nu$, eq. (10) becomes

$$<(\Delta V)^2> = C^2\lambda^\nu U_\nu(\kappa\lambda) \tag{11}$$

where $U_\nu(\kappa\lambda)$ is a slowly varying function such that

$$U_\nu(\kappa\lambda) = 1 \qquad \text{for } \kappa\lambda \longrightarrow \infty$$

and

$$U_\nu(\kappa\lambda) = \text{Const}(\kappa\lambda)^{-\nu} \qquad \text{for } \kappa\lambda \longrightarrow 0$$

A direct estimate of $\kappa\lambda$ can be obtained from the comparison between radio and H_β fluxes of Table 4. Using the equations of Paper II, the total optical depth at H_β is $\tau_\beta \approx 7$ or $\kappa_{H\beta}^{-1} \approx 5$ pc^{-1}. The solution to eq. (11) therefore can be approximated as

$$B(s_1,s_2) = C^2|s_1-s_2|.$$

The solution of eq. (9) in this case is

$$<\sigma_A^2> = \frac{1}{2} C^2\kappa^{-1} + \frac{\beta^2}{2} \tag{12}$$

Equation (12) shows that the fluctuations in profile width observed in 30 Doradus must be due to fluctuations in the optical depth of the nebula. Using eq. (12) with $\kappa_{[OIII]}^{-1}$ equal to $\kappa_{H\beta}^{-1}$ one obtains $<\sigma_A^2> \approx 10$ km sec^{-1} close to

the value of 12 km sec^{-1} given in Table 8.

Since $\kappa^{-1}_{H109\alpha}$ is essentially equal to Λ it is clear from (12) that the H109α line must be broader than the optical recombination lines. Moreover, since κ is proportional to $f(\lambda)$ and thus to κ^{-1}, eq. (12) also predicts that $V_{turb}(H\alpha)$ must be larger than $V_{turb}([OIII]\lambda5007)$ as is observed.

An independent check on the validity of the assumptions which lead to eq. (12) can be obtained by intercomparing the H_α profile width with the width of the [OIII] lines in 30 Doradus. From (12) follows that

$$\frac{f(5007)}{f(H_\alpha)} = \{V^2_{turb}(H_\alpha)-\beta^2_{H\alpha}\}/\{V^2_{turb}([OIII])-\beta^2_{[OIII]}\} .$$

From the data in Table 8, and $\beta^2_{H\alpha}= [f(5007)/f(\alpha)]\beta^2_{[OIII]}$ one gets $f(5007)/f(H\alpha) = 1.52$ in good agreement with the value of 1.44 predicted by Whiteoak's (1966) extinction law (§IIIb).

Consider now the integrated properties of the nebula. Since the mean radial velocities and the profile widths for 30 Doradus are observed to be totally uncorrelated, the overall turbulent velocity is given by

$$V^2_{turb} = 2\langle\sigma^2_A\rangle + 2\langle V^2_A\rangle . \qquad (13)$$

The [OIII] observations of Smith and Weedman give $(2\langle\sigma^2_A\rangle)^{1/2}$ = 17 km sec^{-1} and $(2\langle V^2_A\rangle)^{1/2}$= 20 km sec^{-1}. Thus from (13)

$V_{turb}([OIII])$ = 26 km sec^{-1}, in good agreement with the value of 25 km sec^{-1} derived by Smith and Weedman (1972) from their 120" observations. Similarly, the H_α turbulent velocity is $V_{turb}(H_\alpha)$ = 29 km sec^{-1}.

Using the relation $\langle(V_A-V_B)^2\rangle = C^2\lambda$ for 30 Doradus, it follows that if $\lambda<\Lambda$ then $\langle V_A^2\rangle = C^2\lambda + \langle V_A V_B\rangle$. For 30 Doradus the observed cross correlation term $\langle V_A V_B\rangle$ tends to zero as λ approaches Λ. Thus equation (12) becomes

$$V_{turb}^2 = C^2(\Lambda+\kappa^{-1}). \qquad (14)$$

It one assumes that $\kappa^{-1} = a\Lambda$, eq. (14) becomes $V_{turb}^2 = C^2(1+a)\Lambda$ which is similar to the observed relation

$$V_{turb}^{(2.3\pm0.2)} = \text{Const.}\Lambda$$

established by Melnick (1976a, Paper I) for giant HII regions. The assumption $\kappa^{-1} = a\Lambda$ implies that the volume filling factor of the core of the larger HII regions is smaller than the filling factor of the core of smaller nebulae. This assumption is reasonable and does not contradict the observations of Paper II.

It is not possible at present to establish the origin of the empirical correlation of velocities exhibited in Figure 9. It may by conjectured, however, that the highly supersonic motions observed may be produced by the amplification of galactic shear as a consequence of the

gravitational collapse of the interstellar cloud out of which the HII region formed. This explanation would also account for the large motions observed in the HI cloud surrounding 30 Doradus (and also NGC 604). After the original cloud collapses, it forms an HII region having shear motions of the order

$$\Delta V \simeq (\rho_{HII}/\rho_{IC})^{1/3}\sqrt{\frac{GM}{R}}\ (\Lambda/R)$$

where ρ_{HII} is the density of the HII region and ρ_{IC} is the density of the interstellar cloud which originated the HII region. R is the distance of the HII region to the center of the galaxy of mass M. Using a mass of $10^{10}M_{\odot}$ for the LMC (Burbidge and Burbidge 1975 and references therein) and a distance of 1.6 kpc from the center of the LMC to 30 Doradus, together with a compression factor $(\rho_{HII}/\rho_{IC})^{1/3}\sim 8$, velocities of the order of 24 km sec^{-1} are obtained for Λ = 30 parsecs. Similarly, for the HI cloud in NGC 604 for example, using the observations of Wright (1971) and a compression factor of 3, velocities of the order of 30 km sec^{-1} are obtained, in good agreement with the observations (cf Table 8).

If the motions originate as a consequence of galactic shear, it is to be expected that, if more massive galaxies have steeper rotation curves, they would form more "turbulent" HII regions. Table 9 summarizes the relevant data for the parent galaxies of the HII regions considered in

Paper I. A plot of the average turbulent velocity $\langle V_{turb} \rangle$ of the largest HII regions in these galaxies against the mass of the parent galaxy as determined from rotation curves is presented in Figure 10. It can be seen that, even allowing for uncertainties of factors of 2 or 3 in the masses, there is still a good correlation between the mass of the galaxy and the state of motion of its largest HII regions.

c) Concluding Remarks

The cluster model for giant extragalactic HII regions developed above appears to repeesent well the observations of 30 Doradus. A direct prediction of the model is that the velocity dispersion of the stars imbedded in giant HII regions must be equal to that observed in the nebular gas. Moreover, if a significant fraction of the field O and B stars in galaxies like the LMC, for example, are formed in HII regions, the model predicts that their velocity dispersion should be significantly larger than that of the O and B stars in the Galaxy.

TABLE 1

RESULTS OF THE 65 ARC SEC DIAPHRAGM OBSERVATIONS

SPOT	δx	δy	$\log \frac{H_\alpha}{H_\beta}$	$\log \frac{H_\beta}{H_\gamma}$	$C_{\beta\gamma}(H_\beta)$	$-\log F(H_\beta)^\dagger$
1	-290	+086	0.71	0.42	0.17	10.68
2	-290	-071	0.58	0.43	...	11.02
3	-333	+003	...	...	...	11.03
4	-181	+266	0.58	0.37	...	11.20
5	-181	+108	0.59	0.41	0.10	10.74
6	-110	+195	0.72	0.42	0.17	10.30
7	-110	+037	0.66	0.44	0.34	10.23
8	-176	+003	0.75	0.44	0.24	10.89
9	-038	+086	0.67	0.45	0.29	10.28
10	-038	-071	0.70	0.44	0.34	10.31
11	-137	+015	...	0.54	1.06	10.10
12	-137	-142	...	0.50	0.73	10.93
13	-112	-255	0.38	0.41	0.10	10.88
14	-003	+338	0.70	0.40	0.00	10.67
15	-003	+181	0.67	0.42	0.19	10.59
16	-060	+013	0.79	0.43	0.25	10.82
17	-058	+038	0.72	0.42	0.14	9.93
18	-032	+003	0.70	0.43	0.32	10.20
19	+023	-289	0.57	0.43	0.22	10.85
20	+023	-445	0.63	0.44	0.33	10.17
21	+045	-255	0.30	0.43	0.22	10.87
22	+098	+110	0.47	0.41	0.13	10.39
23	+098	+034	0.66	0.45	0.34	10.22
24	+099	+038	0.73	0.45	0.36	10.48
25	+124	+003	0.68	0.44	0.31	10.54
26	+096	+003	0.72	0.37	...	10.35
27	+166	-175	...	0.42	0.13	10.82
28	+069	-182	0.63	0.34	...	10.95
29	+069	-339	0.63	0.32	...	11.22
30	+192	-263	0.65	0.42	...	11.12
31	+192	-070	0.63	0.43	0.35	10.81
32	+205	+212	0.64	0.40	0.00	10.77
33	+216	+013	0.60	0.37	...	11.14
34	+254	+110	0.54	0.40	0.01	10.97
35	+254	+034	0.65	0.41	0.06	10.69

Table 1 (continued)

RESULTS OF THE 65 ARC SEC DIAPHRAGM OBSERVATIONS

SPOT	δx	δy	$\log\frac{H_\alpha}{H_\beta}$	$\log\frac{H_\beta}{H_\gamma}$	$C_{\beta\gamma}(H_\beta)$	$-\log F(H_\beta)$ †
36	+263	-055	0.65	0.41	0.07	10.76
37	+276	-106	0.55	0.43	0.23	10.79
38	+312	+003	0.03	0.38	...	10.84
39	+323	-175	...	0.41	0.07	11.33
40	+349	-263	0.70	0.44	0.29	10.76
41	+349	-070	0.68	0.43	0.18	10.77
42	+420	-055	0.60	0.40	0.00	10.82
43	+433	-106	0.59	0.42	0.15	11.16

† In ergs cm^{-2} sec^{-1}

TABLE 2

RESULTS OF THE 32.5 ARC SEC OBSERVATIONS

SPOT	$\log\frac{H_\alpha}{H_\beta}$	$\log\frac{H_\beta}{H_\gamma}$	$C_{\alpha\beta}(H_\beta)$	$C_{\beta\gamma}(H_\beta)$	$-\log F(H_\beta)$ †
1	0.56	0.35	0.30	0.16	11.17
2	0.61	0.37	0.47	0.27	11.62
5	0.60	0.34	0.43	0.10	11.35
6	0.54	0.32	0.25	0.00	11.43
7	0.66	0.38	0.61	0.35	10.83
9	0.64	0.34	0.58	0.11	10.89
10	0.64	0.38	0.55	0.35	10.85
11	0.66	0.40	0.62	0.53	10.16
12	0.63	0.36	0.52	0.46	11.72
14	0.56	0.33	0.32	0.00	11.14
15	0.55	0.36	0.29	0.19	11.05
22	0.48	0.33	0.06	0.00	11.51
34	0.55	0.35	0.29	0.13	11.08
37	0.54	0.37	0.27	0.27	11.29
43	0.63	0.36	0.52	0.24	11.47

† In ergs cm^{-2} sec^{-1}

TABLE 3

INTERFEROMETRIC OBSERVATIONS

SPOT[1]	I_0 cts s^{-1}	β_0 km s^{-1}	V_{turb} km s^{-1}	$m_{H\alpha}$
203	20.4	21.7	16.3	$12^m.73$
209	18.7	34.3	31.2	12.10
210	23.0	23.7	18.9	12.30
212	24.7	25.1	20.6	12.25
215	19.5	23.5	18.6	12.54
216	21.6	23.1	18.1	12.40
217	23.1	26.1	21.8	12.18
220	20.7	27.1	23.0	12.24
221	18.7	21.1	15.5	12.76
222	20.4	21.9	16.5	12.62
223	19.1	32.3	28.9	12.25
225	21.4	26.8	22.6	12.34
232	19.4	21.4	15.9	12.61
233	20.9	23.7	18.9	12.45
234	21.9	37.3	34.4	11.71
236	21.2	26.1	21.8	12.27
239	21.5	23.1	18.1	12.35
240	19.8	33.6	30.4	12.01
241	20.6	31.4	27.9	11.80
242	20.0	24.1	19.4	12.49
244	22.7	23.7	18.9	12.50
246	19.7	29.3	25.5	11.92
250	21.9	22.8	17.7	12.35
...†	19.1	30.7	27.1	12.00
...††	26.8	26.6	22.4	12.09
...†††	19.8	25.1	20.6	12.59

[1] The designations of Smith and Weedman (1972) have been used

† $\delta x = -77$; $\delta y = +157$

†† $\delta x = -15$; $\delta y = +73$

††† $\delta x = -103$; $\delta y = +103$

TABLE 4

COMPARISON WITH RADIO CONTINUUM OBSERVATIONS

	D (pc)	I(21)†	$F(H_\beta)$††	$A(H_\beta)$		$S_u(0)$*		N_s		n_e	
				radio	opt	radio	opt	radio	opt	radio	opt
Core:	60	4	8	$3^m.0$	$1^m.3$	87	6	310	62	100	26
Halo:	257	2.5§	12	2.0	0.3	54	8	194	38	4	0.2

† From Mathewson and Healey (1960) in units of 10^{-22} ergs cm^{-2} sec^{-1} Hz^{-1}

†† In units of 10^{-10} ergs cm^{-2} sec^{-1}

§ Includes nonthermal component

* Units of 10^{50} sec^{-1}

TABLE 5

IONIZING STARS IN THE HALO OF 30 DORADUS

Star[1]	Spectral Type	M_V^0	$\log S_u(0)/\pi F_V$	$\log S_u(0)$ sec^{-1}	$Rn_e^{2/3}$ pc cm^{-2}	R_{20} pc
140	OB	-6.5	...	48.0	30	4
138	OB	-5.8	...	48.0	30	4
335	WN+O	-7.3	12.0	50.5	481	65
239	B9I	-8.5	...	47.0	15	2
245	WN7	-6.0	10.9	48.6	72	10
246	WN6	-7.7	11.5	49.9	111	15
248	WN6-7	-6.6	11.3	49.1	68	9
251	WN5	-5.8	12.5	50.1	141	19

[1] From the catalogue of Sanduleak 1968

TABLE 6

IONIZING STARS IN THE CORE OF 30 DORADUS

Star[1]	Spectral Type	$\log S_u(0)/\pi F_V$	M_V^0	M_V^0 Adopted	$\log S_u(0)$ sec^{-1}
133	O8	...	-7.0	...	48.6
134	WN7	10.9	-7.2	-6.8	48.9
135	WN7	10.9	-6.5	-6.8	48.9
136	WN+OB	12.0	-10.2	-10.2	51.4
137	B0.5Ia	...	-7.2	...	46.3
139	WN+OB	12.0	-7.7	-7.7	50.4
140	WN6	11.5	-7.6	-5.8	49.1
141	BO.5	...	-7.6	...	46.3

[1] Star designations by Feast et al. 1960.

TABLE 7

THE REDDENING LAW OF NEBULAR LIGHT

Reddening Law	$f(\beta)/f(\alpha)$	$f(\gamma)/f(\beta)$	R	Δ_u	$\Delta_m(\infty)$
		PREDICTED[1]			
Average O-B stars in the Galaxy (Whitford)	1.58	1.14	3.0	0.39	0.29
Orion Nebula θ^2 Ori C (Whiteoak)	1.69	1.12	3.0	0.30	0.21
	1.35	1.08	5.0	0.30	.24
	1.24	1.06	7.0	0.30	0.26
		OBSERVED			
Orion Nebula[1]	...	...	...	0.23±0.060	
30 Doradus[2]	1.23	1.11	...	0.23±0.06	
Average Giant Extra-galactic HII Regions[3]	1.40	...	...	...	

[1] Münch and Persson 1971

[2] This paper

[3] Melnick 1976b (Paper II)

TABLE 8

KINEMATICAL PROPERTIES OF HII REGIONS

	Orion	30 Doradus	NGC 604
Diameter (pc)	5[1]	257[2]	350[3]
HI Radial Velocity (km/sec)	22[1]	276[5]	-236[6]
HII Radial Velocity (km/sec)	18[1]	269[4]	-241[2]
21 cm line profile width (km/sec)	14[1]	32.5[5]	31.1[6] [7]
Average HII profile widths (V_{turb})			
[OIII]λ5007Å	8.9[1]	17[4]	...
H_α	...	21[2]	25.[illegible][2]
H109α	12.3[8]	32.5[9]	...

[1] Münch 1958

[2] This work

[3] Sandage and Tammann 1975

[4] Smith and Weedman 1972

[5] McGee and Milton 1966

[6] Wright 1970

[7] Rogstad et al. 1976

[8] Reifenstein 1970

[9] Huchtmeier and Churchwell 1970

TABLE 9

OBSERVED PARAMETERS OF THE PARENT GALAXIES

Galaxy	Type[1]	LC[1]	$M/10^{10}M_{\odot}$	$\langle V_{turb} \rangle$
M 33	Sc	III-IV	3.4[2]	23.2[3]
NGC 2366	Ir^{+} or Sc^{+}	IV-V	...	23.0[4]
NGC 2403	Sc	III	5.6[2]	24.3[4]
NGC 4236	SB^{+} or Ir^{+}	IV	...	23.7[4]
M101	Sc	I	16[2]	29.1[3]
NGC 6822	Ir	IV-V	0.15[2]	13.5[4]
LMC	Ir or SBc	III-IV	1.0[5]	20[3,6]

REFERENCES:

[1] Sandage and Tammann 1975

[2] Rogstadt et al. 1967

[3] Smith and Weedman 1972

[4] Melnick 1976

[5] Feast 1964

[6] Smith and Weedman 1971

REFERENCES

Ardesberg, A., Maurice, E., Burnet, J. P., and Prevot, L. 1972, Aston. and Astrophys. Suppl., 6, 249.

Blocklehurst, M. 1971, M.N.R.A.S., 153, 471.

Burgess, A. 1958, M.N.R.A.S., 118, 477.

Burbidge, E. M., and Burbidge, G. R. 1975, in Stars and Stellar Systems, Vol. 9, eds. A. Sandage, M. Sandage, and J. Kristian (Chicago: University of Chicago Press), p. 81.

Castor, J., McCray, R., and Weaver, R. 1975, Ap. J. (Letters), 200, L107.

Conti, P. S., and Leep, G. M. 1974, Ap. J., 193, 113.

Faulkner, D. J., and Aller, L. H. 1964, M.N.R.A.S., 130, 393.

Faulkner, D. J. 1967, M.N.R.A.S., 135, 401.

Feast, M. W., Thackeray, A. D., and Wesselink, A. J. 1960, M.N.R.A.S., 121, 337.

Feast, M. W. 1961, M.N.R.A.S., 122, 1.

Fehrenbach, Ch., and Duflot, M. 1970, Astron. and Astrophys., Special Supplement Series 1.

Gascoigne, S. C. B. 1969, M.N.R.A.S., 146, 1.

Huchtmeier, W. K., and Churchwell, E. 1974, Astron. and Astrophys., 35, 417.

Israel, F. P. 1975, Mittelberg Conference on H II Regions and Related Topics, eds. T. L. Wilson and D. Downes

REFERENCES (CONT'D)

(Heidelberg: Springer-Verlag), p. 288.

Israel, F. P. 1976, Private Communication.

Isserstadt, J. 1975, Astron. and Astrophys. Suppl., 19, 259.

Isserstadt, J., and Meinhardt,R. 1976, M.N.R.A.S., 176, 693.

Kaplan, S. A. 1960, Interstellar Gas Dynamics (Oxford: Pergamon).

Le Marne, A. E. 1968, M.N.R.A.S., 139, 461.

Mathewson, D. S., and Healey, W. R. 1964, The Galaxy and The Magellanic, Clouds, IAU Symp. 20, Canberra, p. 283.

Mathewson, D. S., and Ford, V. L. 1970, Ap. J. (Letters), 60, L43.

McGee, R. X., and Milton, J. A. 1966, Austral. J. Phys., 19, 343.

McGee, R. X., Newton, C. M., and Brooks, J. N. 1974, Austral. J. Phys., 27, 729.

Melnick, J. 1976a, Paper I, Ap. J., in press.

_____. 1976b, Paper II, preprint.

Mezger, P. G., Wilson, T. L., Gardner, F. F., and Milne, D. K. 1970, Astrophys. Letters, 5, 117.

Morton, D. C. 1967, Ap. J., 150, 535.

_____. 1970, Ap. J., 160, 216.

Münch, G. 1958, Revs. Mod. Phys., 30, 1035.

REFERENCES (CONT'D)

Münch, G., and Persson, S. 1971, Ap. J., 165, 241.

Münch, G., and Taylor, K. 1974, Ap. J. (Letters), 192, L93.

Oke, J. B. 1960, Ap. J., 140, 689.

_____. 1965, Ann. Revs. Astron. and Astrophys., Vol. 3.

Oke, J. B., and Schild, R. E. 1970, Ap. J., 161, 1015.

Peimbert, M., and Torres-Peimbert, S. 1974, Ap. J., 193, 327.

Reifenstein, E. C., Wilson, T. L., Burke, B. F., Mezger, P. G., and Altenhoff, W. J. 1970, Astron. and Astrophys., 4, 35.

Rogstad, D. H., Wright, M. C. H., and Lockhart, I. A. 1976, Ap. J., 204, 703.

Sandage, A., and Tammann, G. 1974, Ap. J., 190, 525.

Sanduleak, N. 1968, Contributions of the Cerro Tololo Inter-American Observatory, No. 89.

Searle, L. 1971, Ap. J., 168, 327.

Smith, A. M. 1970, Ap. J., 160, 595.

Smith, L. F. 1968, M.N.R.A.S., 140, 409.

Smith, M., and Weedman, D. W. 1970, Ap. J., 161, 33.

_____. 1971, Ap. J., 169, 271.

_____. 1972, Ap. J., 172, 307.

Snow, T. P., and Morton, D. C. 1976, Ap. J. Suppl., 32, No. 3.

Thuan, T. X. 1975, Ap. J., 198, 307.

REFERENCES (CONT'D)

Terzian, Y. 1974, in Vistas in Astronomy, ed. A. Beer (Oxford: Pergamon), p. 279.

Underhill, A. B. 1968, in Wolf-Rayet Stars, ed. K. B. Gebbie and R. N. Thomas (Washington: National Bureau of Standards), p. 200.

Von Hoerner, S. 1951, Z. Astrophys., 30, 17.

Westerlund, B. E. 1964, The Galaxy and the Magellanic Clouds, IAU Symp. No. 20, Canberra, p. 316.

Westerlund, B. E., and Smith, L. F. 1964, M.N.R.A.S., 128, 311.

Whiteoak, J. B. 1966, Ap. J., 144, 305.

Whitford, A. E. 1958, A. J., 63, 201

Wilson, O. C., Münch, G., Flather, E. M., and Coffeen, M. F. 1959, Ap. J. Suppl., 4, 199, No. 40.

Wright, W. C. H. 1971, Astrophys. Letters, 7, 209.

Figure 1

Red light photograph of the 30 Doradus Nebula taken with the 40-inch (1 meter) telescope at Las Campanas The circles show the positions observed with scanner using 60" apertures. The stars S1 and S2 used to offset the telescope to the observed positions are also indicated on the Figure. The scale of the print is shown on its lower-left corner.

Figure 1

Red light photograph of the 30 Doradus Nebula taken with the 40-inch (1 meter) telescope at Las Campanas The circles show the positions observed with scanner using 60" apertures. The stars S1 and S2 used to offset the telescope to the observed positions are also indicated on the Figure. The scale of the print is shown on its lower-left corner.

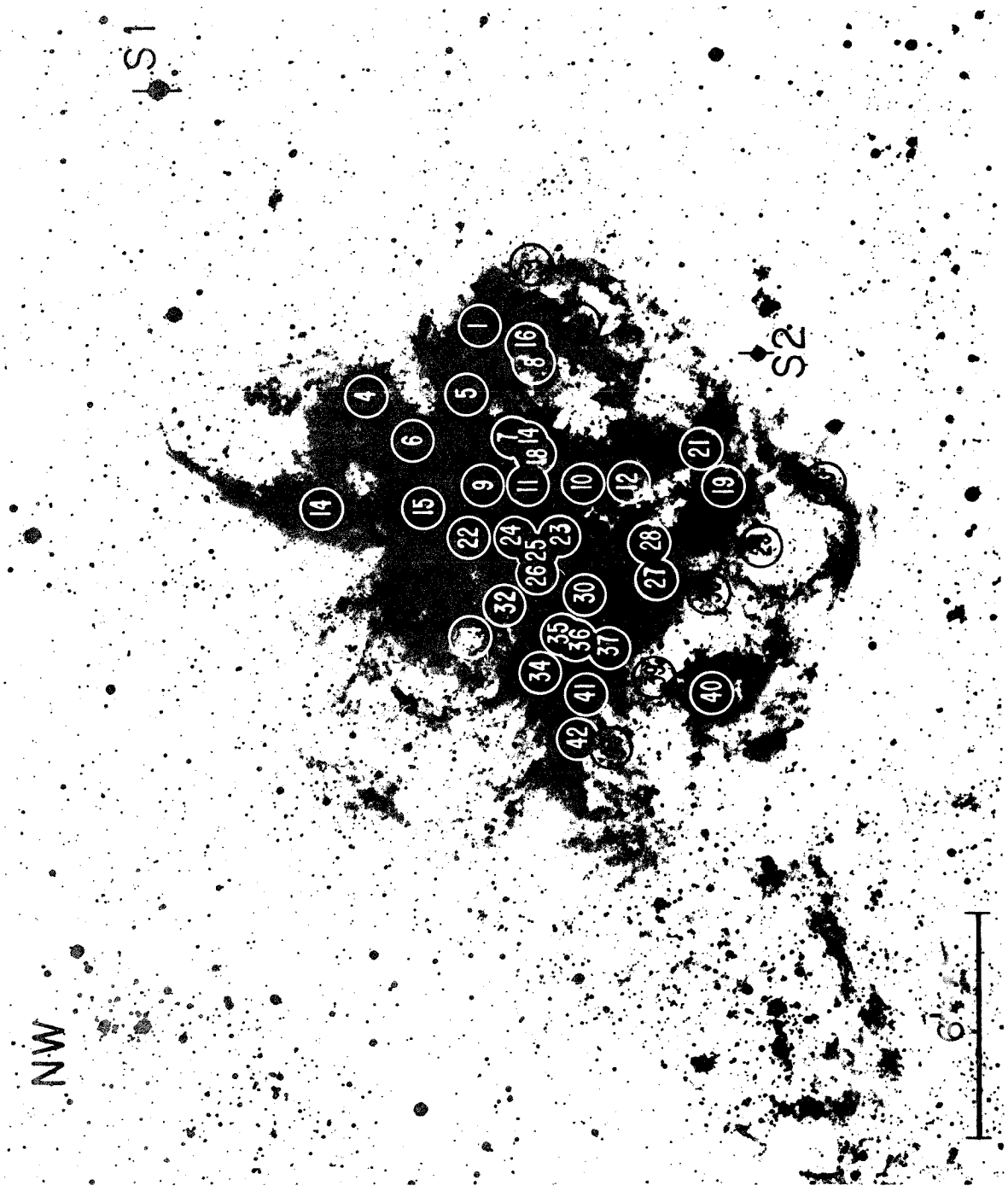
S1
S2
NW
1
2
3
4
5
6
7
8
9
10
11
12
13
14
15
16
17
18
19
20
21
22
23
24
25
26
27
28
29
30
31
32
33
34
35
36
37
38
39
40
41
42

Figure 2

Monochromatic images of 30 Doradus taken with an image tube at the 40-inch (1 meter) Yale telescope at Cerro Tololo. Narrow band interference filters centered at λλ6570 and 6591 were used to compensate for the redishift of the H_α and [NII] lines of the nebula. North is on the upper-right corner and east on the upper-left of the print.

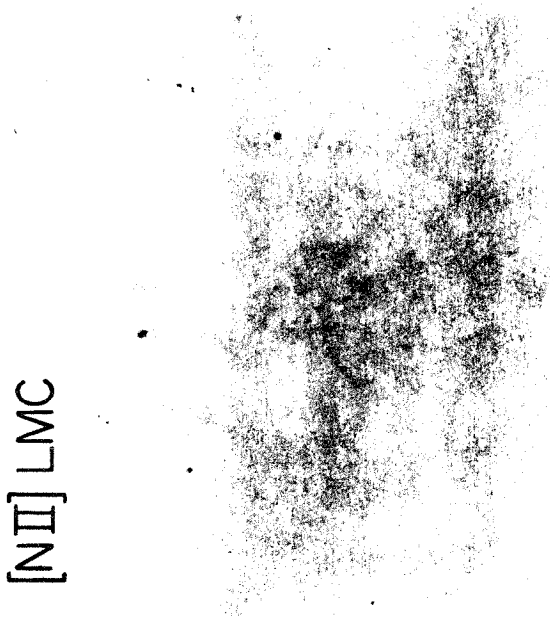
[NII] LMC

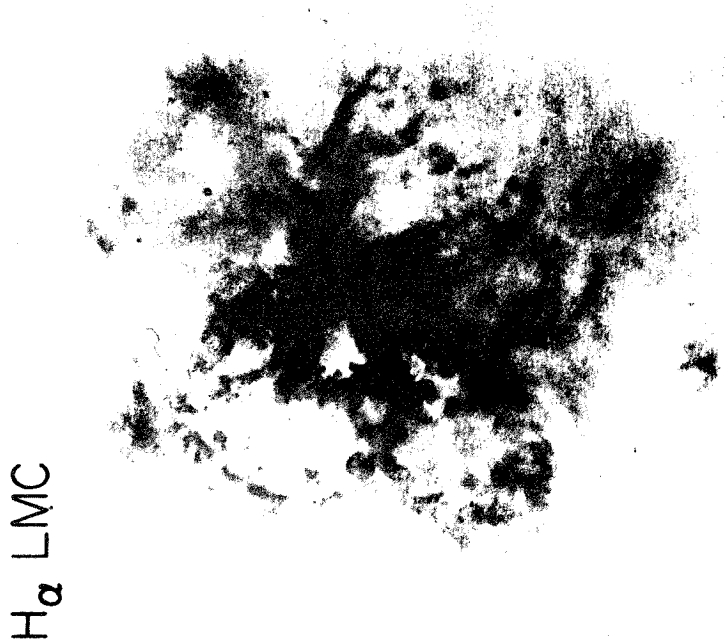
H_α LMC

Figure 3

Visual light photographs of the 30 Doradus Nebula taken with the 40-inch telescope at Las Campanas. The eight O,B and Wolf-Rayet stars in the nebular halo have been identified on the 5-minute phtograph (left). Also marked on that photograph is the central "star" of the nebula R136.

The radius that a uniform HII region with $n_e = 20$ cm^{-3} would have arround each star has been illustrated on the 30-minute photograph (right). Also illustrated are the southern loop L and the compact HII region S discussed in the text. North is on top west is to the right.

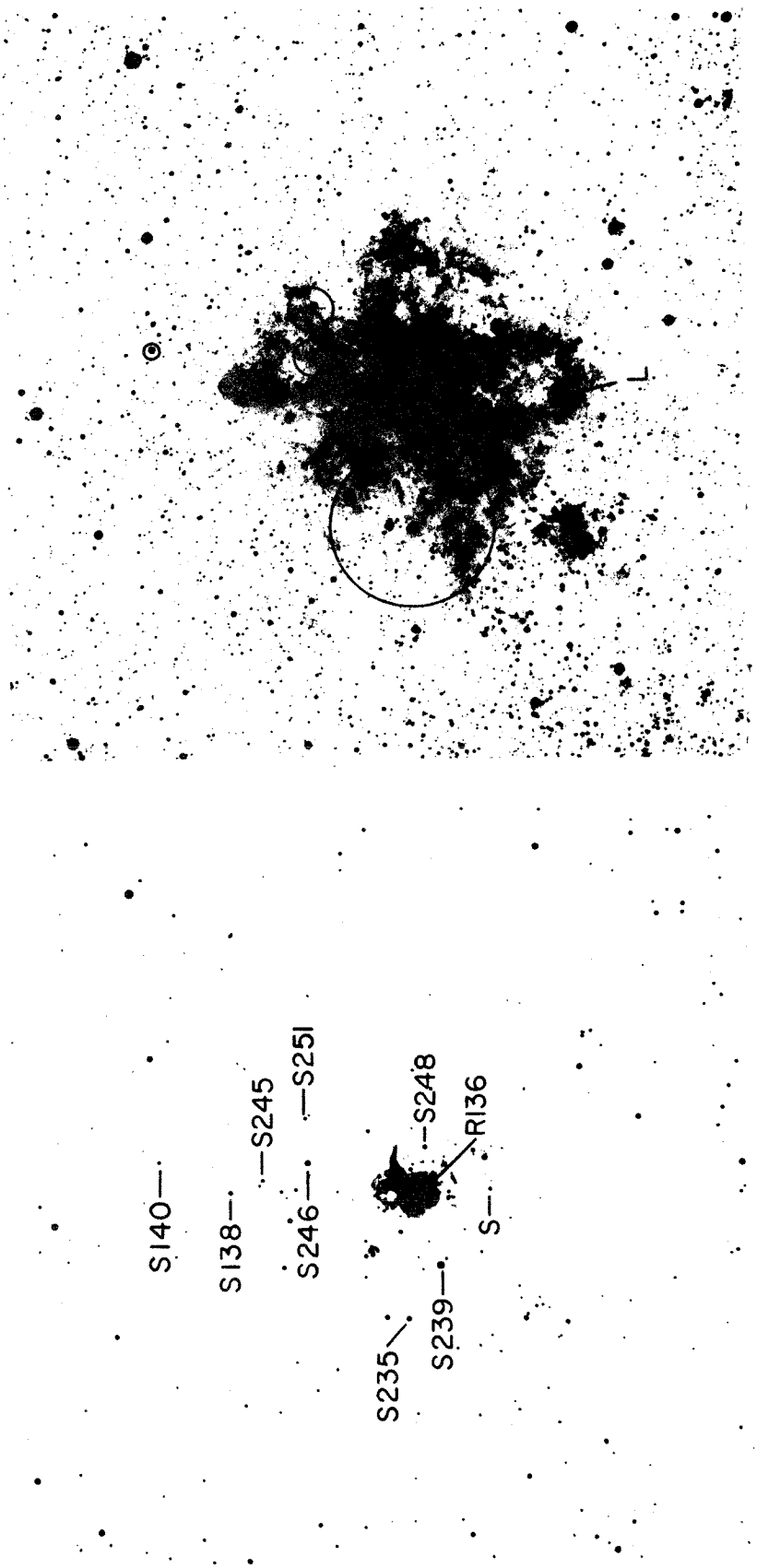
L
S140
S138
S245
S251
S246
S248
R136
S
S239
S235

Figure 4

Monochromatic images of the core of 30 Doradus. The two photographs on the top were taken with an image tube at the Yale 40-inch (1 meter) telescope at Cerro Tololo. The [NII] plate was also reproduced on Figure 2. The OI λ8446 and the [OI]λ6300 images were obtained with a 40-mm magnetically focussed image tube at Las Campanas through interference filters with peak transmissions at λλ6300 and 8450 and half widths of 12 Å and 20 Å (FWHM) respectively. North is on top, east is to the right.

[NII] λ6591

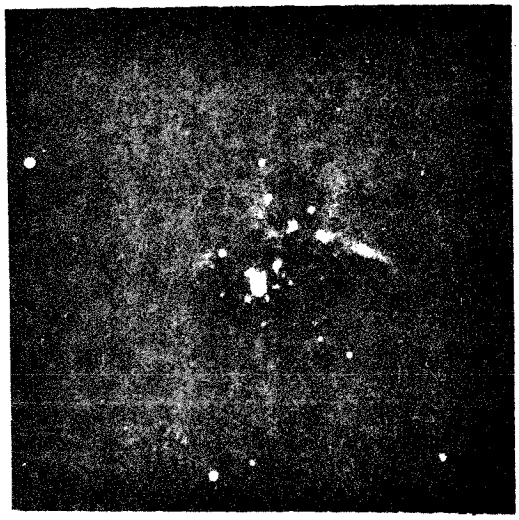

Hα λ6570

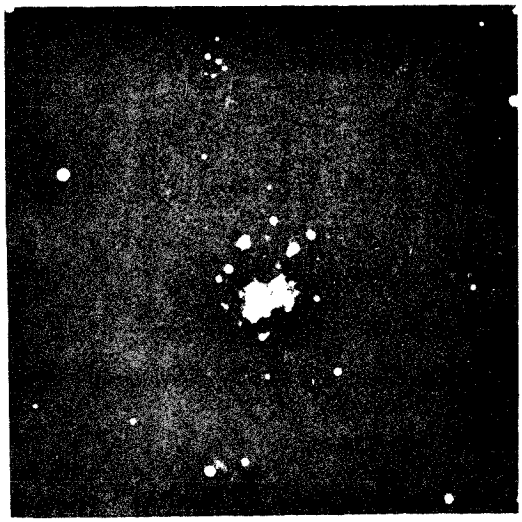

OI λ8446

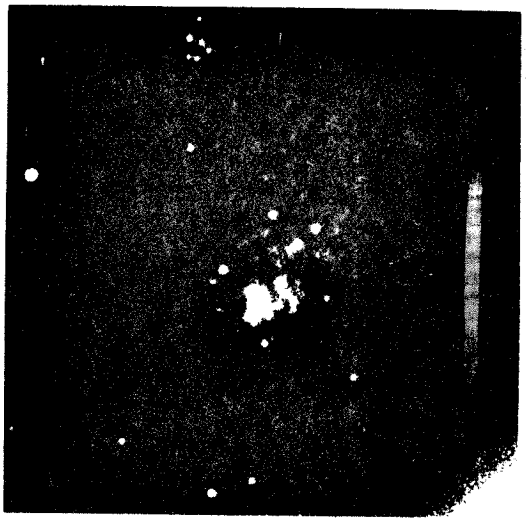

[OI] λ6300

Figure 5

Schematic representation of the reddening distribution in 30 Doradus. The H_β absorption in magnitudes $A(H_\beta) = 2.5C(H_\beta)$ is shown in four intervals represented by different simbols as indicated on the figure.

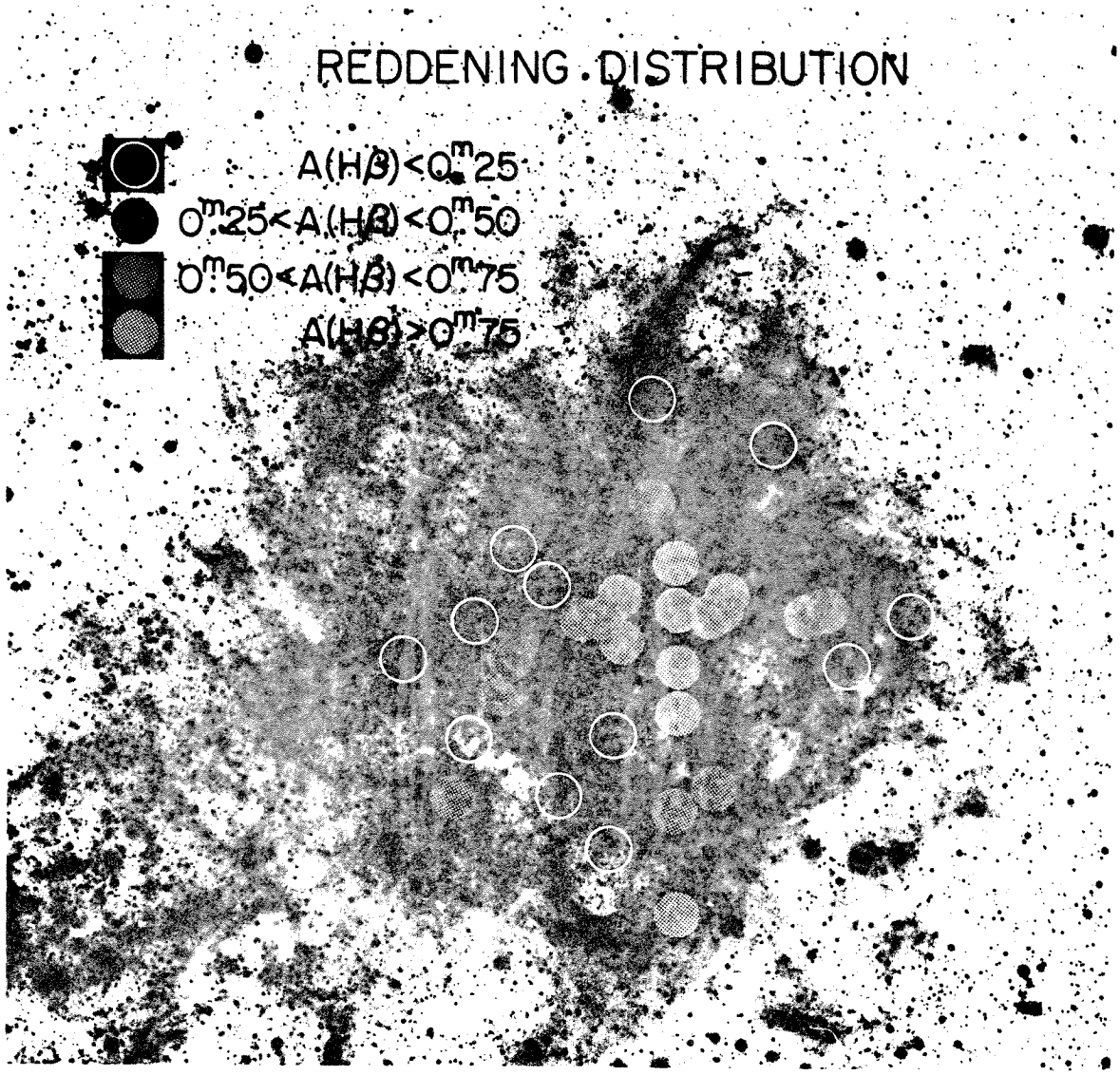
REDDENING DISTRIBUTION
A(Hβ)<0.m25
0.m25<A(Hβ)<0.m50
0.m50<A(Hβ)<0.m75
A(Hβ)>0.m75

Figure 6

Average histogram of the function ϕ defined in section IIIb. An arbitrary normalization has been adopted for the ϕ values.

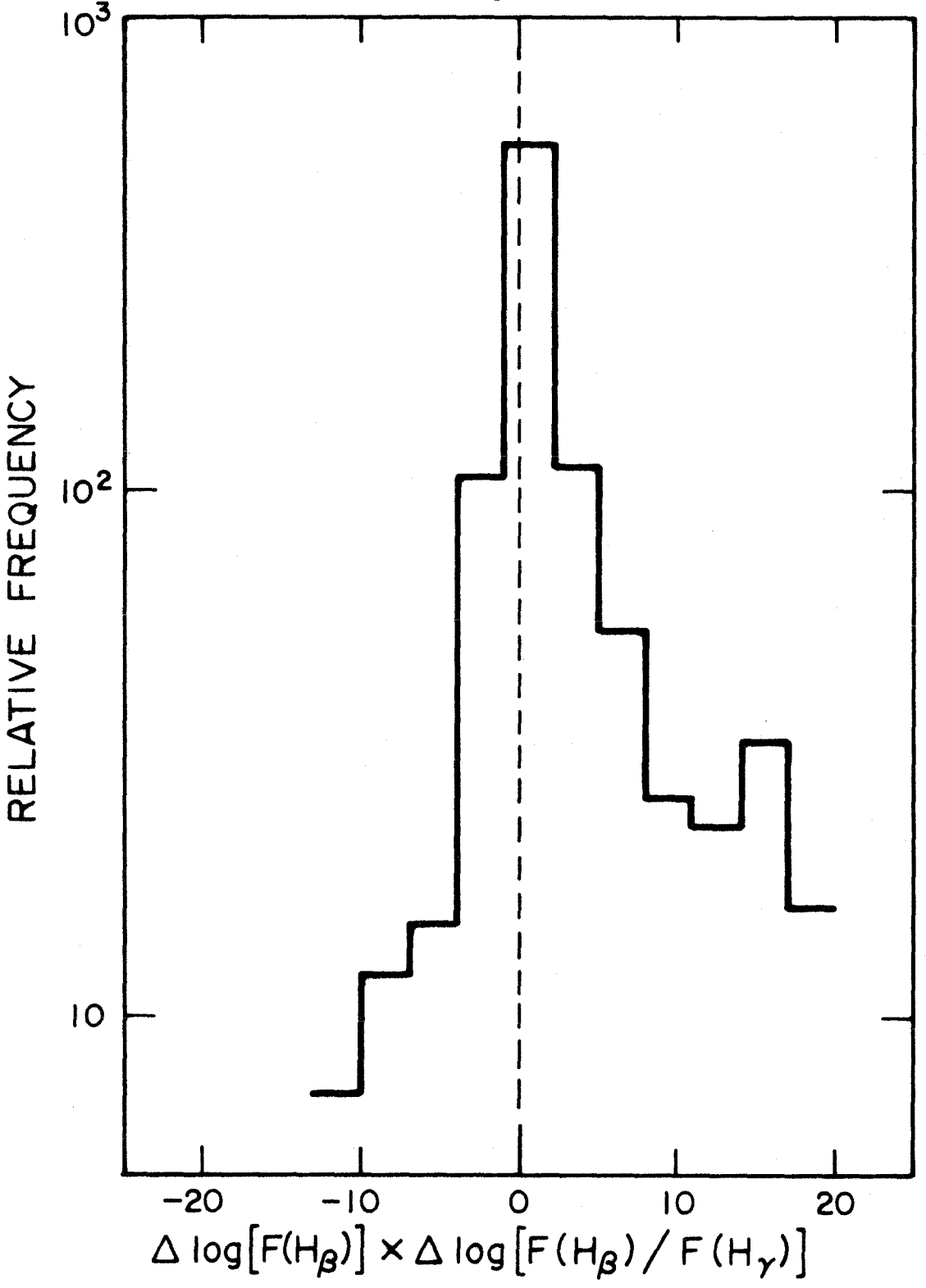
RELATIVE FREQUENCY
10^3
10^2
10
-20
-10
0
10
20
$\Delta \log[F(H_\beta)] \times \Delta \log[F(H_\beta)/F(H_\gamma)]$

Figure 7

Nebular two-color diagram representative of the 32".5 observations. The solid line is a least squares fit to the observed points. The two points labeled Bu and Bl represent the theoretical recombination points of Burgess (1958) and Blocklehurst (1971) respectively.

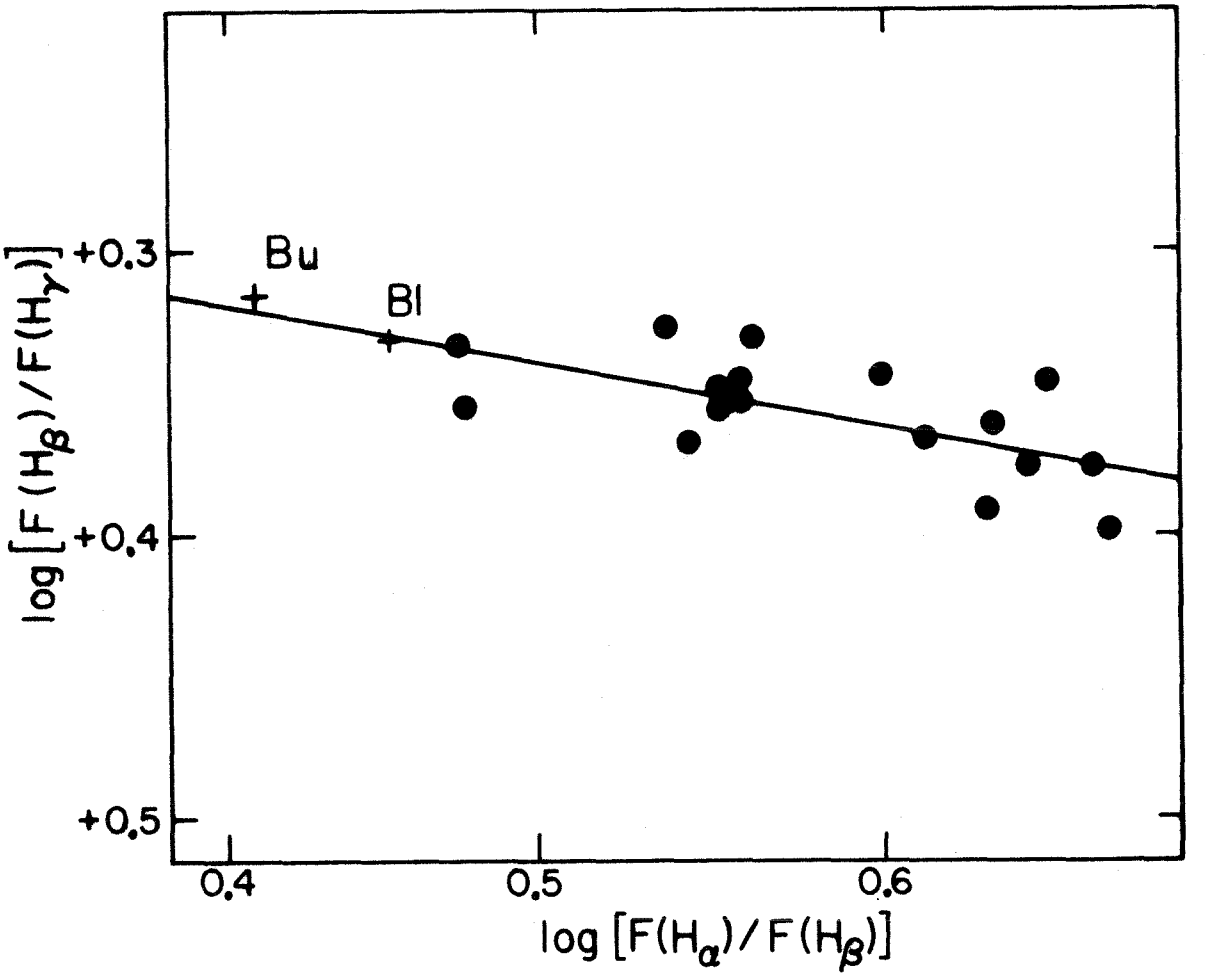
Bu
Bl
+0.3
+0.4
+0.5
0.4
0.5
0.6
log [F(Hβ)/F(Hγ)]
log [F(Hα)/F(Hβ)]

Figure 8

Logarithmic plot of the H_α surface brightness of the 30" spots observed by Smith and Weedman (1972), against the corresponding turbulent velocity, V_{turb}. An arbitrary normalization has been used for the magnitude scale.

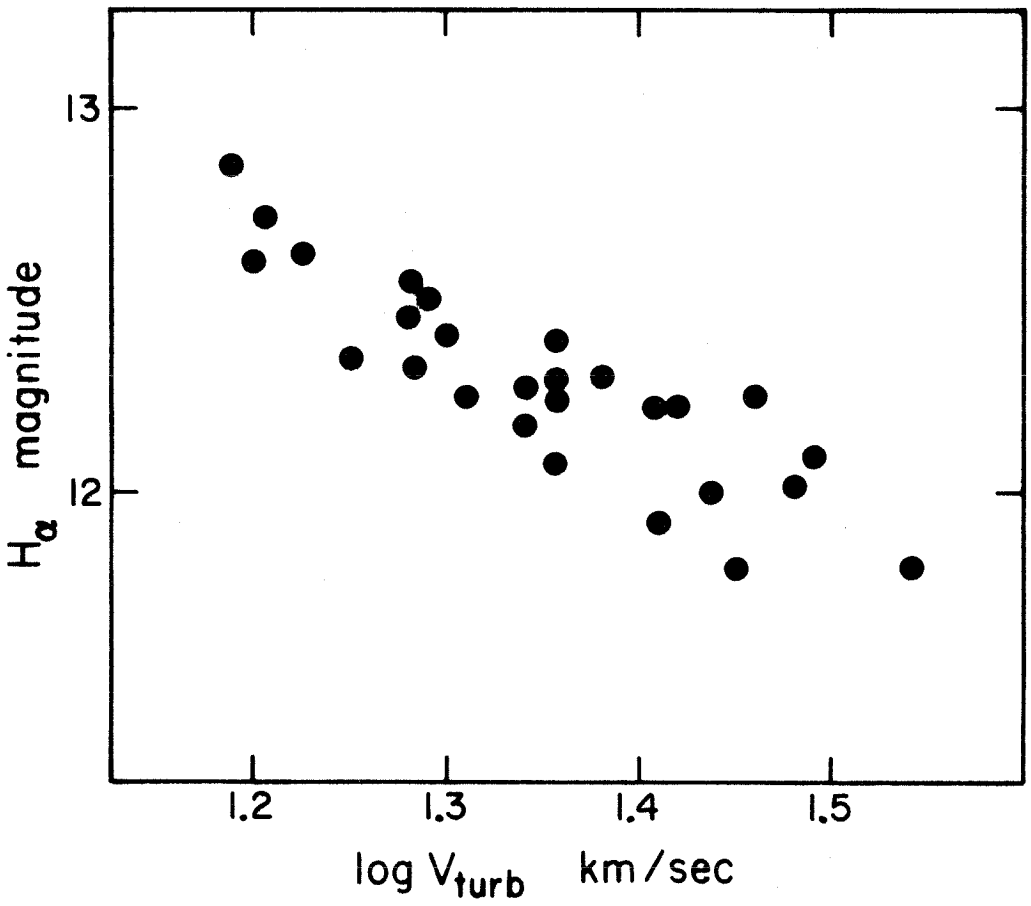
13
12
H_α magnitude
1.2
1.3
1.4
1.5
log V_{turb} km/sec

Figure 9

Correlation between the root-mean-square difference in velocity at two points of the 30 Doradus Nebula and their mutual separation. The solid line represents an eye fit to the observed points.

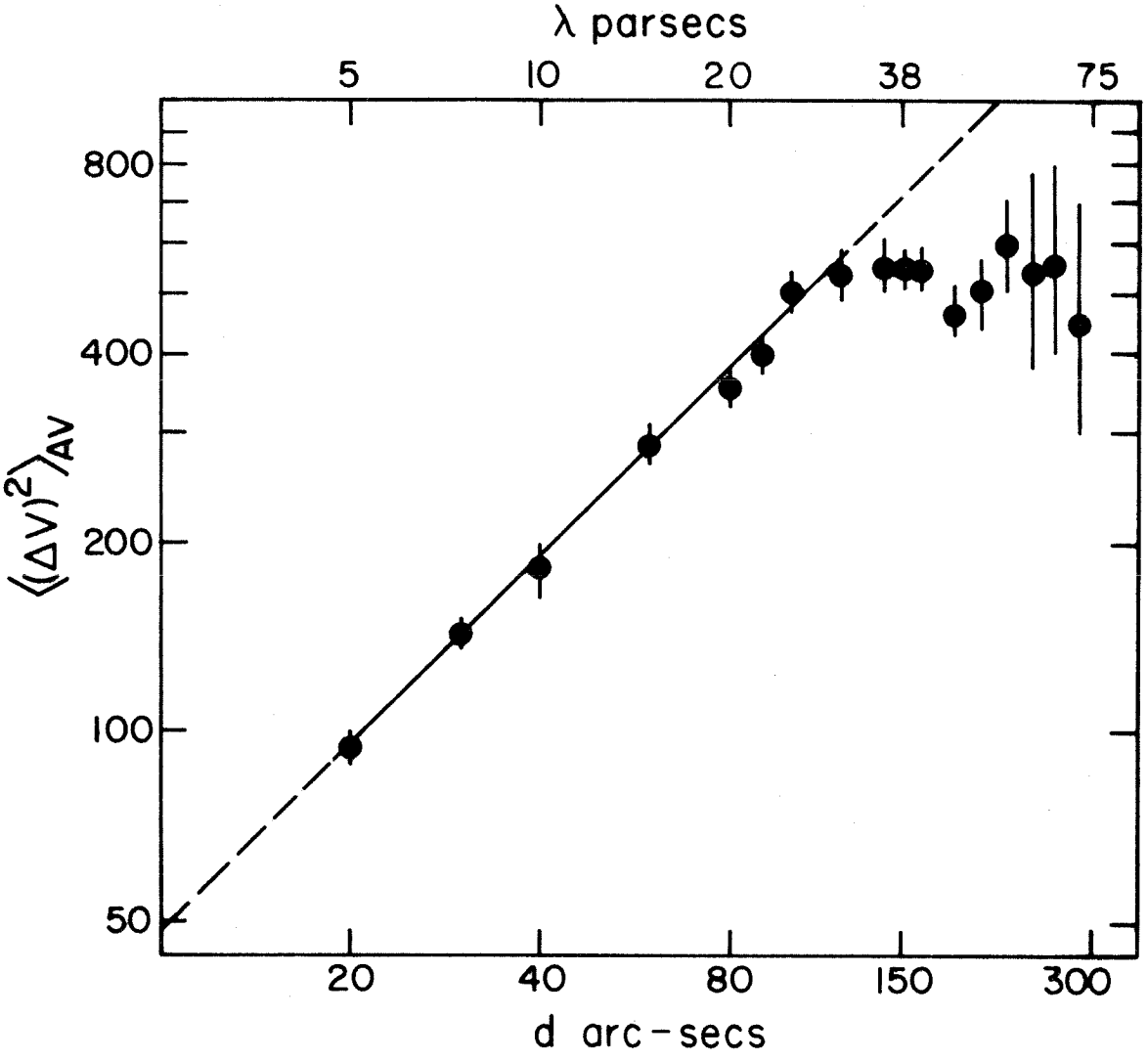
λ parsecs
5
10
20
38
75
800
400
200
100
50
$\langle(\Delta V)^2\rangle_{AV}$
20
40
80
150
300
d arc-secs

Figure 10

Plot of the mean turbulent velocity of the largest HII regions if five spiral and irregular galaxies against the mass of the parent galaxies as determined from rotation curves.

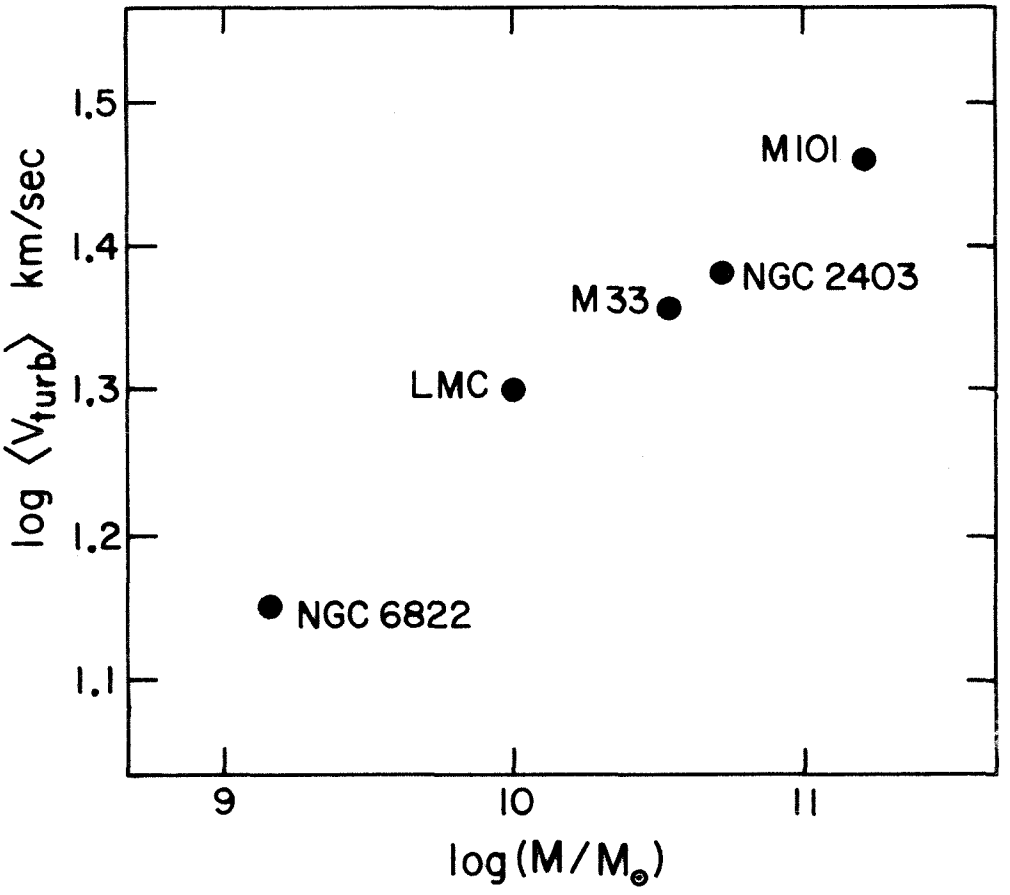
1.5
1.4
1.3
1.2
1.1
log ⟨V_turb⟩ km/sec
M101
NGC 2403
M33
LMC
NGC 6822
9
10
11
log (M/M⊙)